

FACULDADE DE ENGENHARIA DA UNIVERSIDADE DO PORTO



Digital Twin (DT) of a DC-DC converter for Photovoltaic (PV) Applications

José Miguel Dias Braga Lino

Mestrado em Engenharia Eletrotécnica e de Computadores

Supervisor: Rui Esteves Araújo

Second Supervisor: Louelson Costa

November 28, 2022

Resumo

Os conversores DC-DC são uma parte fundamental de qualquer Sistema Fotovoltaico, pois são os responsáveis por aumentar a eficiência da produção de energia pelo sistema. Contudo, estes são também um dos componentes mais susceptíveis a falhas, sendo que em alguns casos estas falhas podem constituir uma ameaça para a segurança do sistema e em casos mais graves, podem mesmo pôr em risco os edifícios e as pessoas que neles se encontram. Por estas razões, a procura de novos e melhores métodos de diagnóstico e identificação de falhas é justificada.

Nesta dissertação, é desenvolvido um algoritmo mais tradicional de diagnóstico de falhas baseado no sinal, como instrumento de comparação para uma abordagem mais ambiciosa, sob a forma de um *Digital Twin*. Ambos os métodos implicam analisar falhas pré-determinadas em sistemas fotovoltaicos e seleccionar as variáveis de diagnóstico mais relevantes para avaliar o comportamento do sistema, a fim de detetar e distinguir falhas. O primeiro algoritmo compara os valores destas variáveis com os valores medidos dois passos de tempo de controlo anteriores no mesmo sistema, enquanto o *Digital Twin* compara os valores do sistema "físico" com os do modelo "gémeo".

Ambos os algoritmos são capazes de identificar correctamente cinco falhas diferentes: Rotura do cabo, falha no algoritmo MPPT, uma falha de curto-circuito no transístor, uma falha de circuito aberto no transístor e uma falha de intermitência. Estas falhas foram modeladas no Matlab Simulink para um conversor DC-DC no sistema PV, enquanto um script de inicialização foi escrito em Matlab para facilitar a mudança de parâmetros e a introdução de falhas no sistema.

Foi inserido ruído branco em cada medição para avaliar a eficiência de cada algoritmo sendo que Precisão, Recall e F1-Score foram as métricas de avaliação escolhidas, com o *Digital Twin* a ser superior em cada um destes valores. Em termos de Precisão, o *Digital Twin* obteve uma pontuação de 68% em comparação com 58% para o algoritmo baseado no sinal, melhor Recall de 92% em comparação com 89% e um F1-Score de 78% em relação a um 70% obtido pelo algoritmo tradicional.

Abstract

DC-DC converters are an integral part of any Photovoltaic System, as they are responsible for increasing the efficiency of energy production by the system. However, these are also one of the components most likely to fail, and in some cases these faults can pose a threat to the safety of the system and, in more serious cases, even put buildings and the people in them at risk. For these reasons, the search for new and improved methods of fault diagnosis and fault identification is warranted.

In this dissertation, a more traditional Signal-Based fault diagnosis algorithm is developed as a comparison tool for a more ambitious approach in the form of a Digital Twin. Both methods involve analysing predetermined faults in photovoltaic systems and selecting the more relevant diagnostic variables to evaluate the behaviour of the system in order to detect and distinguish faults. The first algorithm compares the values in these variables with those measured two control time steps earlier in the same system, while the Digital Twin compares the values in the "physical" system with those in the model "twin".

Both algorithms are capable to correctly identify five different faults: Cable breakage, failure in the MPPT algorithm, a Short-Circuit fault in the transistor, an Open-Circuit fault in the transistor and an Intermittence fault. These faults were modelled in Matlab Simulink for a DC-DC converter in the PV system, while an initialisation script was written in Matlab to facilitate the changing of parameters and introducing faults in the system. White noise was inserted into each measurement to evaluate the strength of each algorithm. Precision, Recall and F1-Score were the chosen metrics of evaluation, with the Digital Twin being superior in each of these values. In terms of Precision, the Digital Twin achieved a score of 0.68 compared to 0.58 for the Signal-Based algorithm, better Recall of 0.92 compared to 0.89 and an F1-Score of 0.78 relative to a 0.7 obtained by the traditional algorithm.

Agradecimentos

A finalização desta dissertação representa o final de uma das etapas mais desafiantes que já alguma vez tive. No entanto, as pessoas que me acompanharam contribuíram (e muito) para que fosse também das mais felizes, e queria por isso mesmo deixar um agradecimento sentido numa tentativa de retribuir tudo aquilo que por mim fizeram.

Em primeiro lugar, quero agradecer à minha família, porque sempre de tudo fizeram para que não me faltasse nada e são o grande motivo por eu ser a pessoa que sou hoje. Ambiciono nunca perder os valores que me foram transmitidos e passá-los àqueles que me rodeiam.

Aos amigos de Civil, por fazerem a chegada à FEUP tão mais fácil e se terem mantido bem presentes até ao ponto de saída.

Aos meus companheiros do Académico. Rimos e chorámos, dentro e fora de campo, estiveram sempre muito presentes na minha vida e deixo-vos por isso mesmo o meu sincero agradecimento.

Aos eletrotos, aos deuses de msin, e aos amigos dos lanches da 13h30, que apesar de em períodos diferentes da jornada, sempre me acompanharam e ajudaram a que todos os serões de estudo passassem num instante.

Aos amigos de Ermesinde, que são também os mais antigos, e que me acompanham em todas as etapas da minha vida. Sei que estarão comigo nas que estarão por vir, e por isso deixo aqui o meu obrigado.

Ao Paulo, que sempre foi o meu parceiro de estudo. Ao Zé, que sempre me acompanhou nesta reta final. Ao Bruninho, que esteve sempre lá quando precisei. Agradeço-vos pelo vosso apoio e companhia, que foi fundamental neste percurso. Sem vocês esta luta teria sido bem mais difícil.

À Fátima e à Suzana, que sempre se disponibilizaram para me ajudar no que fosse preciso e sempre tentaram resolver qualquer problema que eu tivesse.

À Lucie, que nunca me deixou ficar mal, ouviu todas as minhas reclamações como se nada fosse, e foi o meu apoio sempre que precisei, o meu sentido obrigado.

Ao Louelson, que ao longo desta dissertação sempre se mostrou disponível para me ajudar e me esclareceu qualquer questão que tivesse, e ao Prof. Rui Esteves Araújo pela orientação e longas horas de discussão interessantíssimas que tanto me serviu para aprender.

Por fim, gostaria de agradecer a todas as pessoas que fazem parte da comunidade da FEUP que sempre contribuíram para que me sentisse como em casa. Por vezes, foi mesmo aqui onde mais tempo passei, e não fosse a amabilidade e simpatia de todos não teria sido a mesma coisa.

José Lino

“The greatest fear that we face is ourselves.”

Kobe Bryant

Contents

Resumo	iii
1 Introduction	1
1.1 Context	1
1.2 Objectives	2
1.3 Document Structure	2
2 Scientific Background	3
2.1 PV Systems	3
2.2 MPPT Algorithms	5
2.2.1 Perturb and Observe	5
2.2.2 Incremental Conductance	6
2.3 DC-DC Converters	7
2.3.1 Boost Converter	7
2.3.2 Buck Converter	8
2.4 Faults in PV systems	8
2.4.1 Fault Diagnosis Algorithms	9
2.5 Digital Twin Technology	13
3 System and Fault Description	15
3.1 Global System Overview	15
3.2 MATLAB Initialization Script	18
3.3 No Fault Mode	20
3.4 Cable Fault	21
3.5 MPPT Fault	22
3.6 SC gate Fault	23
3.7 OC gate Fault	25
3.8 Intermittence Fault	25
4 Fault Diagnosis Algorithms	29
4.1 Signal-Based Algorithm	29
4.1.1 Cable Fault	31
4.1.2 MPPT Fault	33
4.1.3 SC Fault	33
4.1.4 OC Fault	36
4.1.5 Intermittence fault	42
4.2 Digital Twin	45
4.2.1 Cable Fault	47

4.2.2	MPPT Fault	49
4.2.3	SC Fault	52
4.2.4	OC Fault	52
4.2.5	Intermittence fault	59
5	Algorithm Evaluation	63
5.1	Variable Analysis	63
5.2	Testing of algorithms without undesirable diagnostic variables	65
5.3	Noise Evaluation	68
6	Conclusion and Future Work	73
6.1	Conclusion	73
6.2	Future Work	74
	References	75

List of Figures

2.1	Solar cell model.	3
2.2	I-V Curve of a solar cell.	4
2.3	Micro-grid PV system.	4
2.4	Perturb and Observe algorithm flowchart.	5
2.5	Incremental Conductance algorithm flowchart.	6
2.6	Types of DC-DC converters in PV applications.	7
2.7	Boost Converter for PV Applications.	8
2.8	Buck converter for PV applications.	8
2.9	Classification of the semiconductor fault diagnostic algorithms aimed at DC-DC converters.	11
2.10	Evolution of DT-related studies over the last few years.	13
2.11	Overview of a digital twin approach for fault diagnosis of the complete PV system.	14
3.1	Chosen PV system in its simplest form.	15
3.2	Model of the PV panel UPSolar UP-M310P.	17
3.3	MPPT algorithm.	17
3.4	Values in the boost converter without faults.	20
3.5	Load values without faults.	20
3.6	Final values after 1 second of simulation.	20
3.7	Implementation of the cable fault in Simulink.	21
3.8	PV measurements during Cable fault.	22
3.9	Load measurements during Cable fault.	22
3.10	PV measurements during MPPT fault.	23
3.11	Load measurements during MPPT fault.	23
3.12	Modeled SC Fault in Simulink.	23
3.13	PV measurements during SC fault.	24
3.14	Load measurements during SC fault.	24
3.15	Modeled OC Fault in Simulink.	25
3.16	PV measurements during OC fault.	26
3.17	Load measurements during OC fault.	26
3.18	Influence of intermittence fault.	27
3.19	PV measurements during fault.	27
3.20	Load measurements during fault.	27
4.1	Example of the data study.	30
4.2	Location of OC and SC measurements.	31
4.3	Cable fault algorithm in Simulink.	32
4.4	Duty cycle evolution with $R_{Load}=40\Omega$ for MPPT fault.	33

4.5	MPPT fault algorithm in Simulink.	36
4.6	SC fault algorithm in Simulink.	37
4.7	Implementation of a maximum threshold.	38
4.8	OC fault algorithm in Simulink.	41
4.9	Implementation of the algorithm in Simulink.	44
4.10	Digital Twin in Simulink.	45
4.11	Data study for the DT.	46
4.12	Implementation of cable fault algorithm for DT with fixed irradiance.	47
4.13	Implementation of MPPT fault algorithm for DT with fixed irradiance	51
4.14	Implementation of SC algorithm for DT with fixed load.	56
4.15	Implementation of OC algorithm for DT with fixed irradiance in Simulink.	59
4.16	Implementation of Intermittence fault algorithm in DT with fixed load.	62
5.1	Variable usage in all algorithms	64
5.2	Implementation of OC algorithm with less variables in Simulink	65
5.3	Fault warnings when a Cable fault was introduced without the undesirable diagnostic variables for the Signal-Based algorithm.	66
5.4	Fault warnings when an Intermittence fault was introduced without the undesirable diagnostic variables for the Signal-Based algorithm.	66
5.5	Difference in diagnostic variable V_{PV} with an Intermittence fault in the system.	67
5.6	Fault warnings when an MPPT fault was introduced without the undesirable diagnostic variables for DT with fixed irradiance.	67
5.7	Illustration of the addition of white noise in Simulink.	68
5.8	Confusion Matrix.	71

List of Tables

2.1	Fault events in PV Systems.	10
2.2	Different FD algorithms.	10
2.3	Effects of the increase in Temperature and Irradiance, and the occurrence of a OC Fault.	12
3.1	UPSolar UP-M310P characteristics.	16
3.2	Different simulation modes.	18
4.1	Studied variables.	32
4.2	Chosen time periods.	33
4.3	Simulation results for Cable fault.	34
4.4	Cable fault Signal-Based algorithm	34
4.5	MPPT fault simulation results.	35
4.6	MPPT fault Signal-Based algorithm	35
4.7	SC fault simulation results.	37
4.8	SC fault Signal-Based algorithm.	38
4.9	OC fault simulation results.	39
4.10	OC fault signal-based algorithm.	40
4.11	Intermittence fault simulation results.	42
4.12	Intermittence fault Signal-Based algorithm.	43
4.13	DT simulation paremeters.	47
4.14	Cable fault simulation results.	48
4.15	Cable fault algorithm in DT with fixed irradiance.	48
4.16	Cable fault simulation results with fixed load.	49
4.17	Cable fault algorithm for DT with fixed load.	50
4.18	MPPT fault simulation results for DT with fixed irradiance.	50
4.19	MPPT fault algorithm for DT with fixed irradiance.	51
4.20	MPPT fault simulation results for DT with fixed load.	52
4.21	MPPT fault algorithm in DT with fixed load.	53
4.22	SC fault simulation results for DT with fixed irradiance.	53
4.23	SC fault algorithm for DT with fixed irradiance.	54
4.24	SC fault simulation results for DT with fixed load.	55
4.25	SC fault algorithm in DT with fixed load.	55
4.26	OC fault simulation results for DT with fixed irradiance.	56
4.27	OC fault algorithm for DT with fixed irradiance	57
4.28	OC fault simulation results for DT with fixed load.	58
4.29	OC fault algorithm for DT with fixed load.	58
4.30	Intermittence fault simulation results for DT with fixed irradiance.	60

- 4.31 Intermittence fault algorithm for DT with fixed irradiance. 60
- 4.32 Intermittence fault simulation results for DT with fixed load. 61
- 4.33 Intermittence fault algorithm for DT with fixed load. 61

- 5.1 Variable usage between all algorithms 64
- 5.2 Noise study example. 69
- 5.3 Noise study summary for DT with fixed irradiance. 70
- 5.4 Noise study summary for Signal-Based algorithm. 70
- 5.5 Confusion Matrix for Signal-Based algorithm. 71
- 5.6 Confusion Matrix for DT with fixed irradiance. 71
- 5.7 Comparison between methods of Fault Diagnosis 72

Abbreviations

RES	Renewable Energy Sources
PV	Photovoltaic
MPP	Maximum Power Point
MPPT	Maximum Power Point Tracking
DT	Digital Twin
P&O	Perturb and Observe
PWM	Pulse Width Modulation
OC	Open-Circuit
SC	Short-Circuit
FD	Fault Detection
FI	Fault Identification
NASA	National Aeronautics and Space Administration

Chapter 1

Introduction

1.1 Context

Over the last few years, the investment in renewable energies has been increased mainly due to the environmental concerns associated with the “traditional” ways to generate energy as well as a way to reduce the use of the finite fossil fuels.

Among these renewable energy sources (RES), photovoltaic (PV) power systems are becoming one of the most important types of energy production, making use of the seemingly infinite solar irradiation. It has many advantages over other renewable energy sources because solar radiation is the most available resource, it is easily predictable compared to some other RES, requires little maintenance, does not make any noise [1], and can be used for many different applications (such as residential buildings, space systems, electric vehicles, telecommunications, etc.) [2].

However, PV technology is far from perfect. The conversion efficiency of PV systems is relatively low. Commercial panels have an efficiency of 15-20%, while researchers in the laboratory have been able to achieve a cell efficiency of almost 50% [3].

The other major challenge is associated with the nonlinear characteristic of the I-V curve of solar modules, which leads to the need to use algorithms to determine the maximum power point (MPP) of the curve to optimize energy production. These techniques are called maximum power point tracking (MPPT). These MPPT algorithms are used to control DC-DC converters or DC-AC inverters, an integral part of any PV system that plays a major role in conditioning the energy it generates. They can be used to track the MPP at any load or climatic condition and provide an interface to a DC bus or to an inverter, depending on the topology of the system [4].

Due to its importance for the functioning of the whole process, a digital twin (DT) approach is applied to the converter. A DT is a detailed emulation of a real physical system that uses the maximum amount of available data to continuously predict the outputs and overall health of the system it is trying to emulate [5].

In terms of failure rate, power electronic converters are the most critical part of PV systems. If the DC-DC converter is not able to function properly, it will affect the whole system and can cause it to stop. Electrolytic capacitors and power switches, due to the high exposure to mechanical and

thermal stress, are the most likely components to fail in power converters. For this reason, fault diagnosis will be a major focus of this project.

1.2 Objectives

The objective of this dissertation is to propose, analyse, and validate a digital twin approach of a DC-DC converter for photovoltaic applications capable of detecting and identifying faults, while proving that this approach is better than a traditional signal-based algorithm. To this end, this dissertation has as main objectives:

- Accurately model some of the most relevant faults in a DC-DC converter in photovoltaic systems;
- Develop a capable and accurate signal-based algorithm that detects and identifies the selected faults, as a comparison tool for the main DT;
- Develop a digital twin capable of serving the same purpose as the signal-based algorithm with greater efficiency;
- Validate both methods and verify the premise that the digital twin is superior to the traditional signal-based algorithm.

1.3 Document Structure

This document is divided into 3 main parts. First, Chapter 2 describes a summary of the research conducted prior to the actual realisation of the project. Some of the work in this area is also examined and briefly described.

Then, Chapters 3 and 4 describe the procedures for each of the algorithms developed, with Chapter 3 being a brief introduction to the system and its faults, and Chapter 4 describing the core of the work.

Finally, Chapter 5 evaluates the work using some chosen metrics, with conclusions drawn from this work presented in Chapter 6.

Chapter 2

Scientific Background

2.1 PV Systems

PV systems are responsible for converting solar radiation into electrical energy. This is done using PV modules, which consist of PV cells that are quite small and typically produce about 1 or 2 Watts of power. These cells are made of semiconductor materials that when exposed to light, absorb its energy and transfer it to the negatively charged electrons in the material. Afterwards, the electrons will flow through the material as electrical current, being extracted through conductive metal contacts [6].

The energy generated by PV modules is nonlinear, as shown by the I-V curve in Figure 2.2. Its behaviour depends on solar irradiance and temperature and always has a MPP located at the “knee” of the curve. Since solar irradiance and temperature are subject to change, the MPP also changes. Therefore, MPPT algorithms are necessary to optimise solar power generation [7].

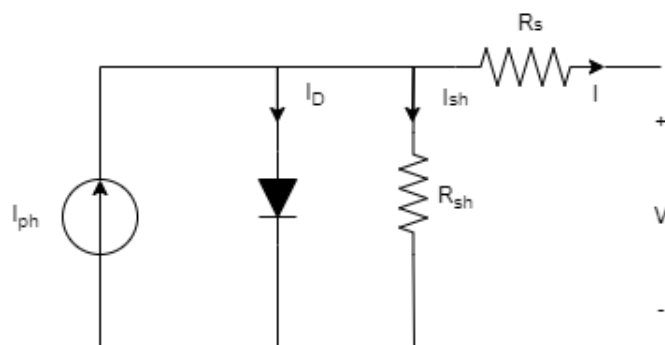


Figure 2.1: Solar cell model.

The operation of a PV panel can be modelled by an electric circuit shown in Figure 2.1. It consists of a photoelectric current source, a diode, and two resistors that model the voltage and current losses in the process [8].

Besides the modules, a PV system consists of many different components. The basic electronic principles and elements are the same, but depending on the type of system, the topology changes

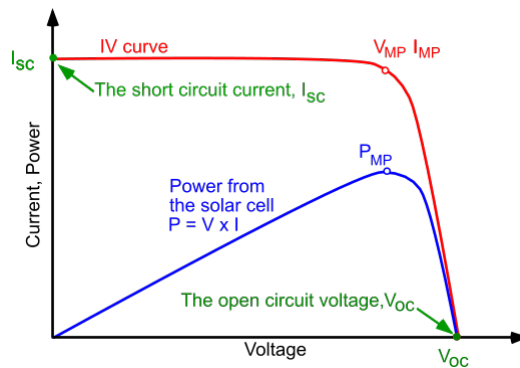


Figure 2.2: I-V Curve of a solar cell.

according to its use.

There are three main types of PV systems: standalone, grid-connected systems, and hybrid systems. As the name suggests, the main difference between standalone and grid-connected systems is that the former are not connected to the grid and are instead linked to a load or batteries for energy storage. Grid-connected systems, on the other hand, use DC-AC converters to connect the system to the grid. Hybrid systems make use of not only solar power but also other types of energy such as wind or gas. This additional component usually means they require a more sophisticated type of control than the other two.

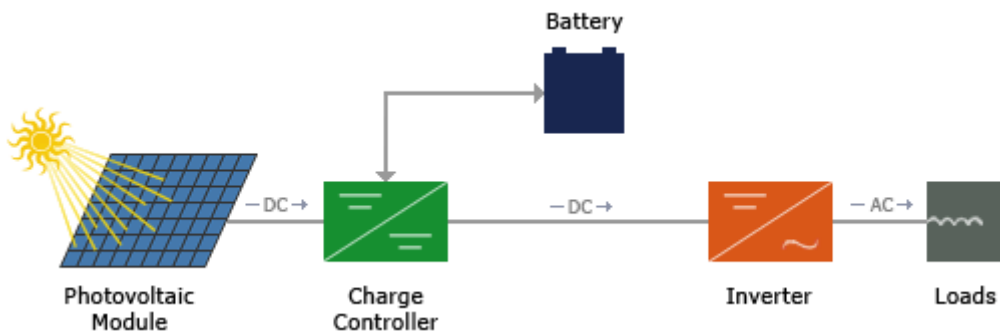


Figure 2.3: Micro-grid PV system [9].

In general, a PV system is composed by the following components:

- A PV array of PV panels to convert solar radiation into photoelectric current;
- A DC-DC converter, to maximize the power produced with the MPPT control and/or to adjust the voltage to a suitable value for the inverter (if that is the case of the system);
- A DC-AC converter, to supply the power to an AC load or grid;
- The system controller, that implements the MPPT algorithm on the DC-DC converter and controls the DC-AC converter;
- If necessary, a transformer, to adjust the voltage to a value suitable for the grid and to protect the PV system from some types of faults.

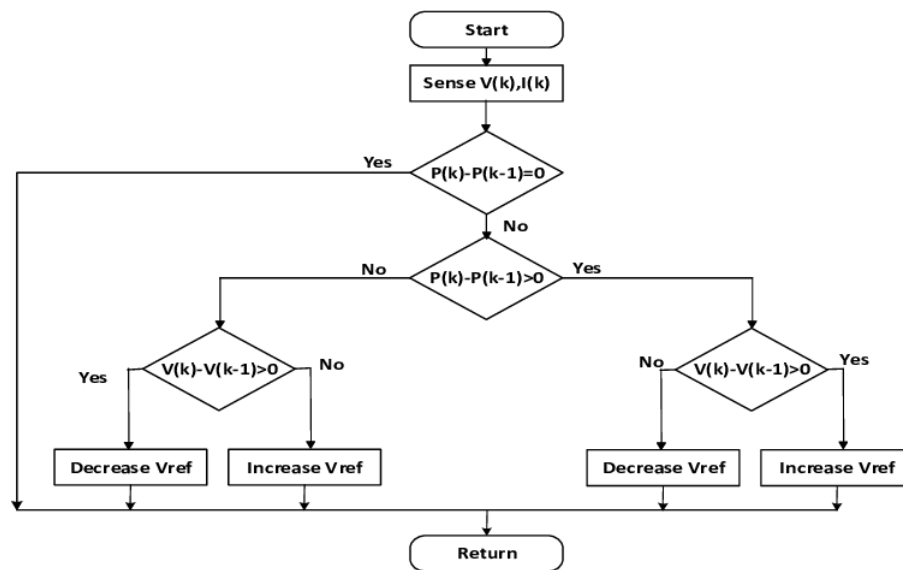


Figure 2.4: Perturb and Observe algorithm flowchart.

2.2 MPPT Algorithms

Photovoltaic energy production is not linear and changes over time, depending on several factors such as solar radiation, temperature, and shadow. Therefore, MPPT algorithms are responsible for determining the duty cycle of the DC-DC converter in order to achieve optimal power production. In this type of algorithms, the convergence speed is one of the most important factors as it helps to improve the overall system reliability, power extraction and efficiency [1]. This can be achieved by many different types of algorithms, some of which are analysed in this report.

2.2.1 Perturb and Observe

The Perturb and Observe (P&O) method is one of the simplest MPPT algorithms and also one of the most commonly used. One of its greatest advantages is this balance between simplicity and performance, and the fact that it does not require knowledge of PV generator characteristics or consideration of weather variables such as solar radiation or temperature. It is also easy to implement with analogue and digital circuits, but lacks the speed and adaptability sometimes required to track fast transients under volatile weather conditions [1]. The P&O algorithm samples both the current and voltage of the PV array and calculates the PV output power and power change using these sampled values. If a particular change (perturbation) results in optimized output power, then the perturbation is performed by changing the duty cycle of the DC-DC converter. This process is repeated until the MPP is reached. The tracker does not operate continuously, and by changing the step size it is possible to compromise between accuracy and speed. [1, 10] The flowchart of the P&O process can be seen in Figure 2.4.

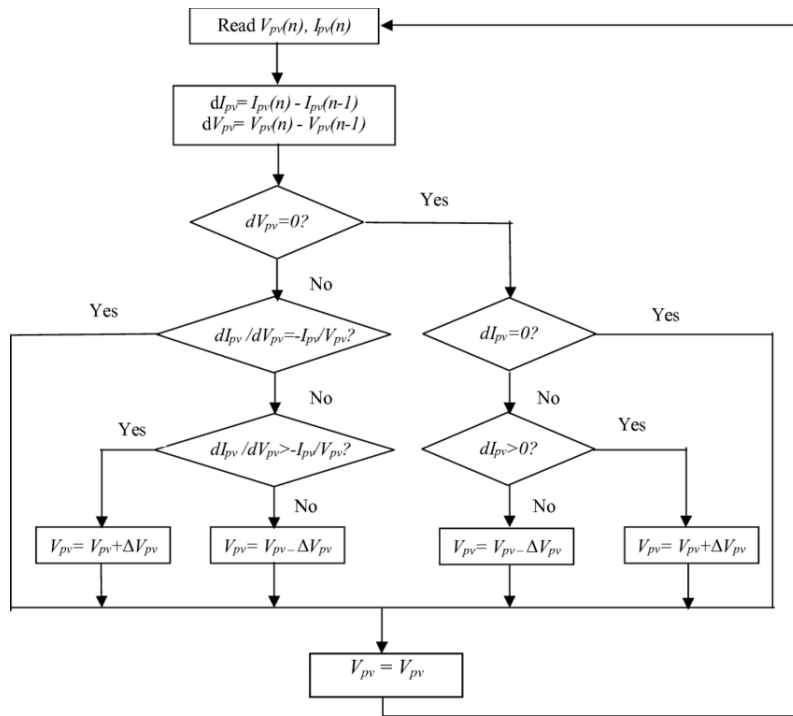


Figure 2.5: Incremental Conductance algorithm flowchart.

2.2.2 Incremental Conductance

The incremental conductance method is based on the assumption that the derivative of the power curve at the MPP is zero. If the slope is negative, the MPP lies on the right side of the last analysed position and if it is positive, on the left side. Depending on this slope, the PV voltage is changed accordingly by changing the duty cycle of the converter, as shown on the flowchart in Figure 2.5.

This is a fast and dynamic method that requires high sampling rates and does not depend on weather conditions. While difficult and expensive to implement, recent developments in micro-controller technology have mitigated this impact.

2.3 DC-DC Converters

A DC-DC converter is an electronic circuit responsible for regulating the voltage/current of a DC source from one level to another desired one. They can be either isolated or non-isolated. Isolated power converters, as the name implies, isolate the input from the output by physically separating the two circuits having no direct conduction path between the two parts of the circuit. This is called galvanic isolation and is usually accomplished with the use of a transformer. A non-isolated converter has a single circuit where current is able to flow directly between the input and output.

Within each type, there are many different converter topologies, and the ones used in PV applications are the ones shown in Figure 2.6 [11].

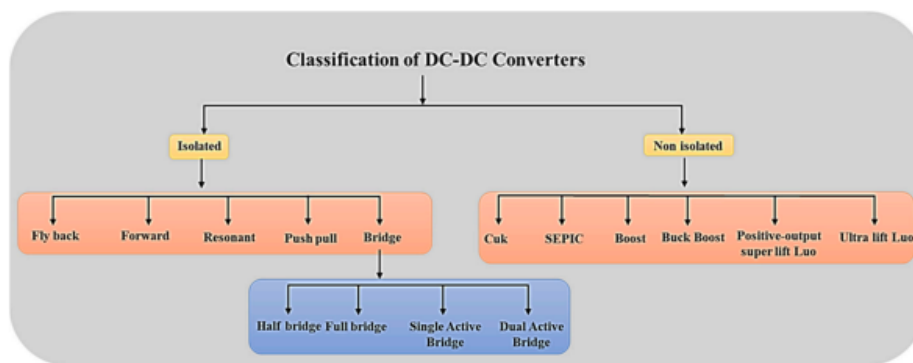


Figure 2.6: Types of DC-DC converters in PV applications [11].

2.3.1 Boost Converter

The boost converter is a non-isolated converter that, as the name implies, has a higher output voltage than the input voltage. A picture of a boost converter used in PV applications is shown in Figure 2.7. In its simplest form, it consists of a source, a diode, an inductor, a capacitor, and a switch. When the switch is closed, current flows through the inductor and stores energy in its magnetic field. No further current flows through the circuit as the impedance of the rest of the circuit is higher than the zero resistance offered by the short circuit created by the closing of the switch.

When the switch is open, the inductor releases the stored energy and acts as another source in conjunction with the actual input source, increasing the output voltage. The switch is usually controlled by pulse-width modulation (PWM). Most often, MOSFETs or IGBTs are used instead of a switch to be able to sustain high frequency switching, having a better response to high demand control. In PV applications, MPPT is applied to this converter acting on its duty cycle accordingly and it is used to enhance the power production of the system.

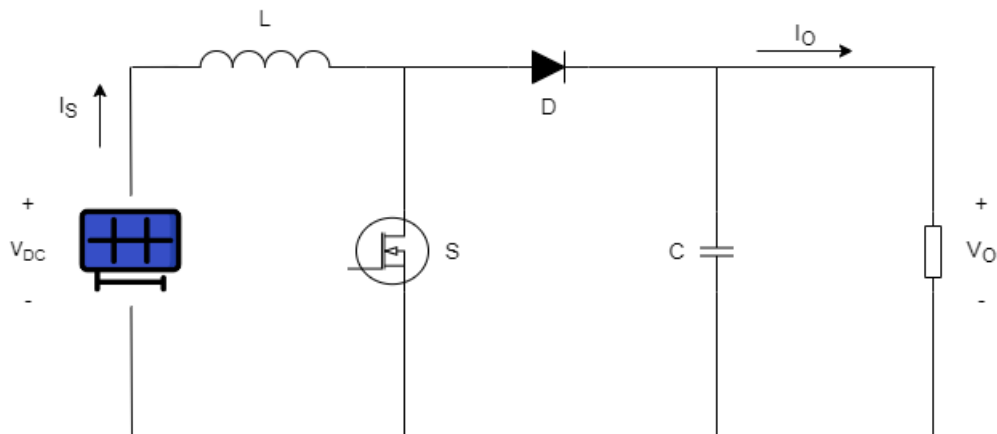


Figure 2.7: Boost Converter for PV Applications.

2.3.2 Buck Converter

The Buck converter operates in contrast to the boost converter, i.e., the output voltage is lower than the input voltage. It is also a non-isolated converter and is composed by the same electronic components, only in a different arrangement, as shown in Figure 2.8. In PV applications, it is usually used to connect systems to a load or batteries with lower voltage [11].

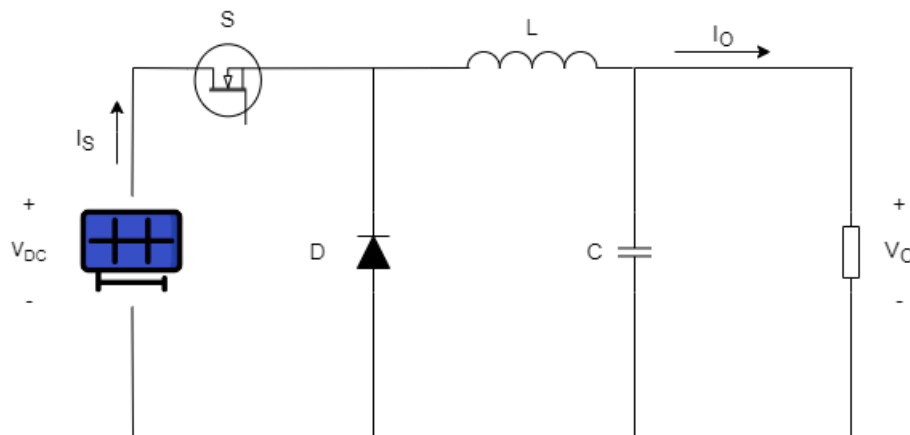


Figure 2.8: Buck converter for PV applications.

2.4 Faults in PV systems

Due to a variety of factors, such as the high number of power electronic converters, complex installation, aging, manufacturer defects, extreme weather conditions, etc., PV systems are prone to a number of faults. The recent increase in demand and complexity of these systems is accompanied by the need to ensure system safety and faultless functioning, as some faults can not only result in a less efficient system, but also endanger the safety of buildings and the people in it. For this reason, investments in fast and reliable fault diagnostic algorithms are of great importance and

have attracted the attention of many researchers in recent years. In a PV system, most faults occur either in the PV panels, power converters, or in the electrical sensors [5].

Faults in DC-DC converters are most likely in these systems as power switches and electrolytic capacitors are subjected to high mechanical and thermal stresses, as in many other power applications. In this project, focus will go through this type of faults. Failure of the converter will result in a less efficient system, as the MPPT algorithm is key to optimising power production and in some cases a fault may lead to system stoppage.

The converter failures caused by semiconductor faults account for 21% of total power converter failures [2]. According to the work done in [12], it was concluded that semiconductor and soldering joints failures in power devices account for 34% of power electronic system faults.

A fault in this component can be classified as either an open-circuit (OC) or a short-circuit (SC) fault.

OC faults are usually the result of wire lifting, gate driver faults, or soldering break and do not pose a real threat to the overall health of the system. However, they significantly degrade the efficiency of the overall system and can be detrimental to the converter if not quickly detected and corrected, underscoring the importance of reliable fault diagnostic algorithms [13].

SC faults pose a real threat and must be detected and corrected within a few microseconds. Integrated SC fault protection is standard practise in power switches but some factors such as the non-linear characteristics of the PV module, shading, the operation of the MPPT algorithm, and the blocking diodes in the PV array can limit the action of these components [14].

As reported in the work done by Jain [15], faults in PV systems are classified into 3 types based on their occurrence: PV panels, power converters, and electrical sensors.

In terms of PV panel faults these can occur due to shading, cell breakage, bypass diode failures, interconnection faults, PID, PV shunt and series resistance, etc.

Electrical sensor faults are related to errors in reading voltage and current values through the system. In the author's project, these types of faults were the easiest and quickest to detect.

Table 1 summarizes some of the faults that can occur in a PV system, as per [15].

2.4.1 Fault Diagnosis Algorithms

In order to increase the safety, efficiency and reliability of PV systems, fault diagnosis algorithms have been studied in detail. These algorithms must not only be able to detect the presence of a fault, but also identify the type of fault. Signaling the occurrence of a fault is called fault detection (FD), while distinguishing between faults is called fault identification (FI) composing the fault diagnosis algorithm.

There are also some algorithms that are able to combine the FD and FI phases, depending on the diagnostic variables selected and the capabilities of the chosen algorithm.

Current algorithms for commercial PV monitoring are typically unable to identify the type of fault, require high bandwidth and additional central processing units, and introduce additional latency in diagnosing system performance and faults [7].

Table 2.1: Fault events in PV Systems [15].

Fault type	Fault Event
PV Panel	Soiling, Continuous partial shading Mild cells breakage Bypass diode failures Continuous severe partial shading Severe cells breakage Interconnect faults PID PV shunt and series resistance faults
Power Converter	Open circuit switch fault Short circuit switch fault MPPT algorithm failure
Electrical sensor	Fault in I_L sensor Fault in I_{Load} sensor Fault in I_{pv} sensor Fault in $V_{C_{in}}$ sensor Fault in $V_{C_{out}}$ sensor Fault in V_{pv} sensor

Table 2.2: Different FD algorithms.

Reference	Algorithm type	Method
[15]	Model-Based	Mathematical modulization of both the DC-DC converter and a fault signature library
[13]	Signal-Based	Analysis of the derivative of input current for the intervals with the maximum number of on-state switches
[4]	Signal-Based	Analysis of the increase/decrease of some parameters in the occurrence of a fault
[16]	Signal-Based	Comparison between a new Unified Switch Fault Diagnosis with two separate fault detection algorithms working in parallel

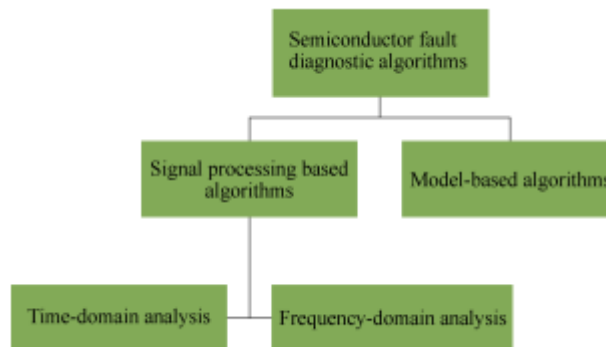


Figure 2.9: Classification of the semiconductor fault diagnostic algorithms aimed at DC-DC converters.

While there is no standard classification scheme for the types of algorithms used to diagnose semiconductor faults in DC-DC converters, according to Bento et al. [13], a possible scheme based on the information required to implement the algorithm is as shown in Figure 2.9.

Most algorithms used in DC-DC converter fault diagnosis are categorized as "signal processing algorithms". They obtain fault signatures based on a few selected values called diagnostic variables, which are collected in real time. Diagnosis is based solely on these fault signatures, which depend on the evolution of these diagnostic variables in the event of a fault. An alternative method is "model-based algorithms," in which a predetermined modulation of the converter is used to diagnose the state of the converter. These types of algorithms have higher robustness against false fault alarms [13].

An example of a possible approach is the one taken by [4] as a Fault Tolerant DC-DC boost converter for a PV system. This approach is based on a signal processing algorithm. In this case, additional components are required (at least two inductances and two capacitors in the input capacitor bank) and the PV array must have an even number of PV modules association. It also requires two additional sensors to determine the input current and voltage for each division of the PV modules, as these values are essential for diagnosing a OC fault with this method.

Fundamentally, the circuit is analysed in different states: healthy, faulty and rebuilt state. As explained earlier, in the occurrence of a OC fault, the circuit will stop functioning shortly, and this transient state between the fault and total failure is deeply analysed in detail in this study by Eunice. However, further studies were needed since the I-V curve of a solar panel is directly influenced by the temperature and irradiance, which change frequently during the course of a day and must not be confused with a fault. These can be easily distinguished as the conclusions obtained were pretty distinct. The effects on cell voltage, current and power are summarised in Table 2.3.

As so, by monitoring the changes in input current, voltage and power, an FD algorithm can be obtained. This was also the chosen approach for the design of the DT, while many other variables were evaluated also evaluated depending on the type of fault that occurred in the system.

Table 2.3: Effects of the increase in Temperature and Irradiance, and the occurrence of a OC Fault [4].

	Voltage	Current	Power
Temperature	Decrease	Increase	Decrease
Irradiation	Increase	Increase	Increase
OC Fault Occurrence	Increase	Decrease	Decrease

This same work by Eunice is also able to distinguish where the fault occurred, i.e. it is able to tell which power switch of the pair has a faulty behaviour.

Bento's work is an example of a different approach to fault diagnosis. Although it is also a signal-processing algorithm, the FD process is different from that of Eunice. The theoretical analysis is quite similar: analysing the circuit during healthy, faulty and recovery state. In this particular case, the input current was chosen as the parameter for evaluating the presence of OC faults in the system. Following the assumption of equal components in all converter phases, the derivative of the input current was determined for each interval of a switching period, which forms the basis for all operation.

This particular algorithm focuses on the periods in which the maximum number of switches are operating in the ON-state. The definition of a gap was between the rising edge of the PWM signal finishing with the subsequent falling edge. While healthy, on the healthy state, the derivative of the input current is always positive according to the assumptions in this study.

After an open-circuit fault in a switch, no current flows through it, and as so, the phase current decreases linearly until reaching zero-phase current, according to the mathematical study done by [13]. In this scenario, the derivative of the current will logically be negative for most cases, with some exceptions that do not affect the FD of the algorithm, as the derivative is negative during the transient state immediately after the fault.

A comparison is made between the absolute value of the input current measured at the beginning and end of the interval (rising and falling edge of the PWM signal). If the switch is healthy, then the difference between $I_{in}(\text{Falling})$ and $I_{in}(\text{Rising})$ should be positive. Since this is not a sufficiently reliable method, the diagnostic variable is normalised to compensate for non-linearities such as load transients in converter operation.

In this sense, the normalised difference of I_{in} should always be positive under healthy operation, with a threshold of -0.5 defined as the criterion for issuing a fault alarm.

While this algorithm has its limitations due to the high computational effort and the associated higher costs, this analysis of the input current during precisely defined time periods represents a new and effective way to define OC faults in DC converters.

2.5 Digital Twin Technology

The concept of the digital twin has evolved steadily over the years. It first appeared in the National Aeronautics and Space Administration's (NASA) Apollo program in the 1970s, when a replica spacecraft was created on Earth to emulate the system status on Earth while the mission was underway. This was the first "twin" application, later defined by Michael Grieves in 2003 as a "virtual digital representation equivalent to physical products" [17]. The development of DT technology did not progress until the year 2012, when NASA redefined the term: "A digital twin is an integrated multiphysics, multiscale, probabilistic simulation of an as-built vehicle or system that uses the best available physical models, sensor updates, fleet history, etc" [5]. Definitions may vary depending on the application domain. Therefore, it is challenging to find a general definition for every field. However, it is generally defined as a realistic and sophisticated emulation of a physical system that predicts its status and outputs in real time, and enabling interaction between both physical and digital twins.

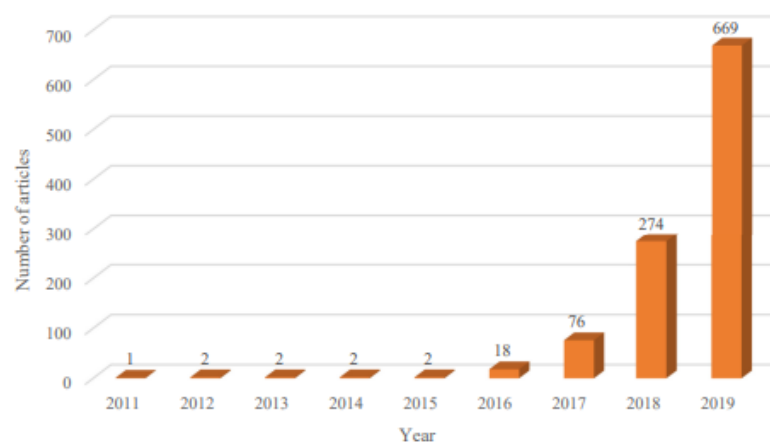


Figure 2.10: Evolution of DT-related studies over the last few years [17].

The emergence of this technology can be seen in the increase of academic papers from Google Scholar on DT-related studies, as shown in Figure 2.10 [17], but also in the financial investment and strategic planning of some of the leading manufacturing countries. In China, DT has become a key component of the Made in China 2025 plan in line with the development and application of a cyber-physical system (CPS), which aims to develop intelligent control systems; Industry 4.0, which is a German high-tech strategy, requires CPS as one of the four main components to predict and optimize a production system in real time; Market Research Future predicts that the market of DT will reach 35 billion USD by 2025; Bitkom stated that the gross German market value of DT can be increased by a cumulative 267 billion euros cumulatively by 2025 after introducing Industry 4.0. [17].

The use of DT in power electronics is relatively new. Using a DT in PV systems with a focus on power electronics is a novel approach that enables improvement in power generation by supporting operation and maintenance with critical analysis that would otherwise be quite difficult

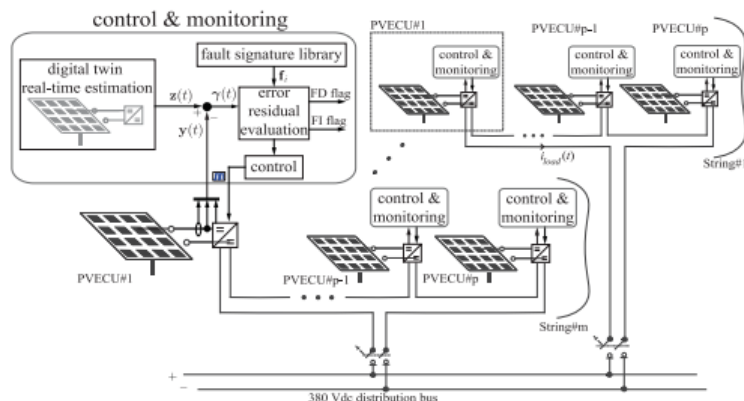


Figure 2.11: Overview of a digital twin approach for fault diagnosis of the complete PV system [15].

without a DT. The improvement is achieved by enhancing the performance of the system's power electronics components, more specifically the DC-DC converter.

While this technology has not been explored in depth when applied to power electronics, one particular project by Jain et al. [15] developed a digital twin for fault diagnosis in a distributed power electronic based PV system. In this project, the design, development and experimental validation were carried out and it is studied in detail in this report due to its relevance.

The proposed approach performs fault diagnosis of each individual PVECU and enhances the dependability of the overall PV system. A model-based DT is developed for each PVECU. An error residual vector is generated by comparing the outputs of the DT with the outputs of the physical twin. Analytic valuation of the error residual vector enables to FD and FI.

Figure 2.11 shows the control and monitoring phase, where the DT takes action. Here, fault diagnosis and control is performed on a single computing platform. It is important to emphasise that the fault signature library seen in the figure contains previously studied knowledge about possible fault events and is an ensemble of analytically computed fault signatures. In this project, the digital twin estimator outputs the PV current and voltage as well as a state vector, making use of previously derived mathematical equations.

For FD, as mentioned earlier, a residual error vector is created that compares the estimate from the DT with the actual physical output. In a fault-free scenario, this vector will be close to zero, with small variations due to analytical estimation errors, discretization errors, and system noise. To protect against false alarms and these deviations, a threshold must be chosen. The FD flag is triggered when the modulus of the deviation vector is higher than the predefined threshold.

Each type of fault will imply a different evolution of the residual error vector in the fault space. To determine this direction, the vector is normalized to a unity vector. After a fault event, an L^2 inner product is computed between the residual error vector and each member of the fault signature library. In order to FI, these inner products are calculated and the maximum value of these products is searched. The product with the highest value will be the cause of the fault, i.e. the fault signature within the library is identified.

Chapter 3

System and Fault Description

The digital twin should be able to detect the occurrence of faults, distinguishing them by type. The system is capable of operating in 6 different modes, having 5 different faults and a no fault mode. Therefore, some types of faults were chosen as the most relevant ones for DC-DC converters for this project.

In this chapter we will first look further into the chosen converter topology and its components, the MATLAB script developed to initialise the system and a deeper look at each of the chosen faults to be detected by the system.

3.1 Global System Overview

The converter topology chosen for this project is a conventional DC-DC boost converter. This is a non-isolated converter, which is quite common in PV applications and is also one of the simplest designs. It has a great relation between efficiency and cost.

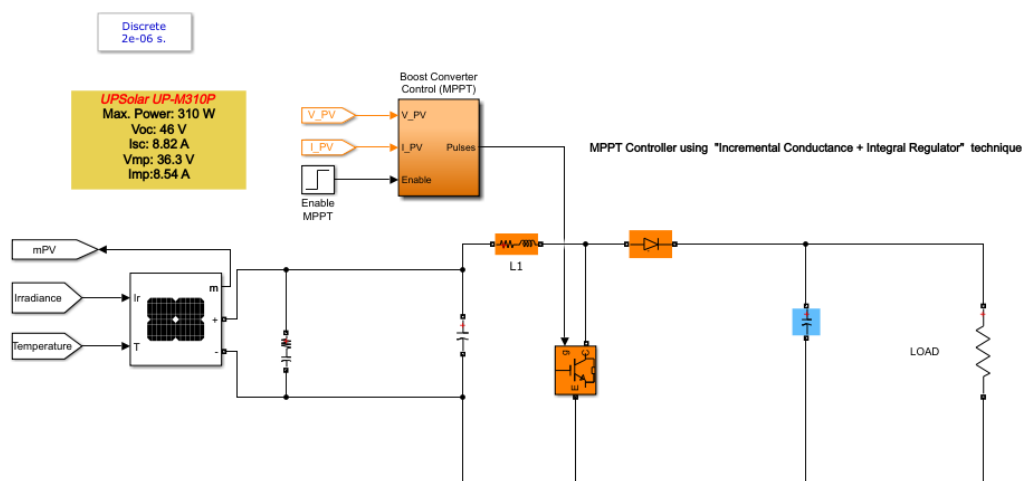


Figure 3.1: Chosen PV system in its simplest form.

Table 3.1: UPSolar UP-M310P characteristics [18].

Maximum Power	310 W
Cells per module	72
Open Circuit Voltage	46 V
Short Circuit Current	8.82 A
Voltage at MPP	36.3 V
Current at MPP	8.54 A
Temperature coefficient of Voc	-0.3442 %/C°
Temperature coefficient of Isc	0.030102 %/C°

Normally, a Digital Twin should be an exact emulation of a real physical system. In this case, since there is no real system to emulate, there is no exact system to be replicated. As so, there is more freedom within the parameters, always with the aim that the project is as versatile as possible while remaining efficient and cost-effective in case there is a desire to adapt this work to a real physical system.

As can be seen in Figure 3.1, the system started with a solar panel connected to a boost converter controlled by an MPPT algorithm, which then supplies a load. This load is just a resistor whose value is not fixed in order to obtain the versatility mentioned earlier.

The solar panel chosen was the UPSolar UP-M310P, as it is one of the models available in both the INESC TEC laboratories and the MATLAB Simulink library for solar panels. The modelling of the solar panel was left unchanged as it was done by Mathworks. Figure 3.2 shows the model circuit of the solar panel. During the work, it was maintained 3 series connected panels with 1 parallel string. The specifications of the said panel according to its datasheet [18] are shown in Table 3.1.

The boost converter is controlled by the Incremental Conductance + Internal Regulator MPPT algorithm. The function of the Internal regulator is to minimise the error and the Incremental Conductance algorithm works as explained in Chapter 2. This algorithm also comes from the Mathworks library and has not been modified. Its operation is shown in the Figure 3.3.

3 parameters were defined: the minimum and maximum value of the duty cycle, and its initial value. A minimum of 0.1 and a maximum of 0.9 were set as threshold values, as values close to 1 and 0 are not common in non-simulation environments. The initial values should be as close as possible to the ideal point. The average of some common loads was calculated, which is at the chosen value of 0.4.

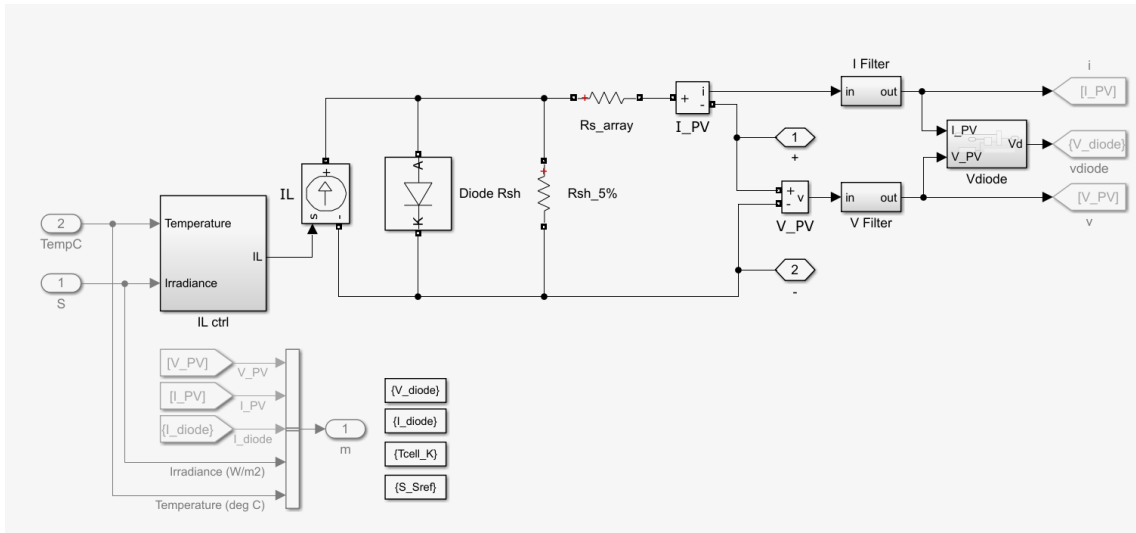


Figure 3.2: Model of the PV panel UPSolar UP-M310P.

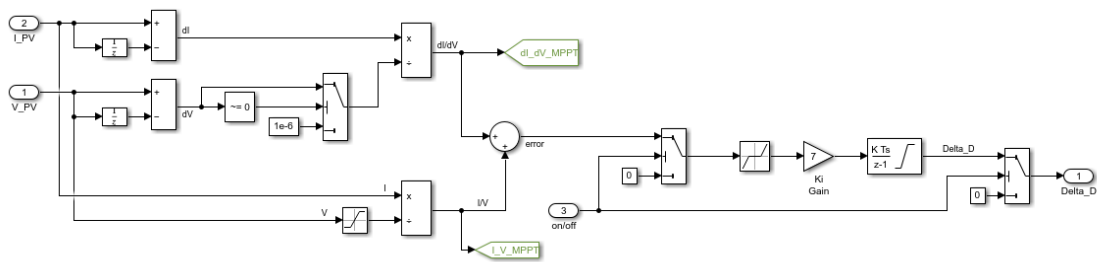


Figure 3.3: MPPT algorithm.

3.2 MATLAB Initialization Script

During this project a lot of simulation work was done, and in order to facilitate the changing of parameters and do some calculations, an initialisation script was created in MATLAB.

It starts by setting some parameters such as the total simulation time, the number of series and parallel panel modules, the control and power time steps, and so on. These were almost always constant and rarely changed.

Afterwards, the script prompts the user to enter two parameters: the load resistance and the simulation mode. There are 6 different simulation modes, as can be seen in Table 3.2. An excerpt from the script is also shown.

The script automatically runs the simulation so no further action is needed in Simulink.

Table 3.2: Different simulation modes.

Input Number	Mode of Simulation
0	No fault mode
1	Cable fault
2	MPPT algorithm fault
3	SC gate fault
4	OC gate fault
5	Intermittence fault

```

1  % PV modules
2
3
4  Irradiance = 1000;
5
6  Ns_modules = 3;
7  Np_modules = 1;
8
9  % Load
10
11 load_ask= "Insert load value (between 20 and 50):"; %works between 17 ...
    and 58
12 Rload = input(load_ask);
13 fsw = 10e3;
14
15 %Inductor
16 L1=5e-3;
17
18 % Capacitors
19 C_In = 22e-6;
20 C_Out = 22e-6;
21
22 % Time steps
23 Ts_Power = 1e-6;

```

```
24 Ts_Control = 100e-6;
25
26 %Insert Fault
27
28 fault_type = 0;
29 OC_switch = 1;
30 SC_switch = 0;
31 mppt_switch = 1;
32 cable_switch = 1;
33 IT_switch = 0;
34
35 prompt= "Insert type of fault:";
36 disp('0-No Fault, 1-Cable Fault, 2-MPPT Fault, 3- SC gate fault, 4- OC ...
      gate fault, 5- Gate intermittence fault;')
37 fault_type = input(prompt);
38
39 switch fault_type
40     case 0
41         disp('No Fault mode')
42     case 1
43         cable_switch = 0;
44         disp('Fault introduced in PV cable')
45     case 2
46         mppt_switch = 0;
47         disp('Fault introduced in MPPT control')
48     case 3
49         SC_switch = 1;
50         disp('SC Fault introduced in gate')
51     case 4
52         OC_switch = 0;
53         disp('OC Fault introduced in gate')
54     case 5
55         IT_switch = 1;
56         disp('Intermittence Fault introduced in gate')
57 end
58
59 disp('Running Simulation')
60 sim("PV_System_wt_DT.slx")
```

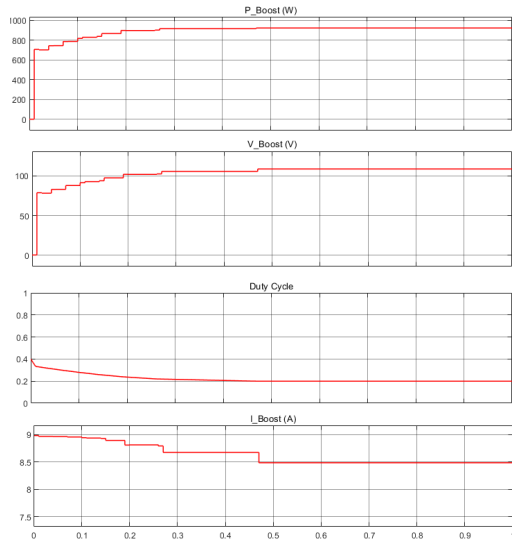


Figure 3.4: Values in the boost converter without faults.

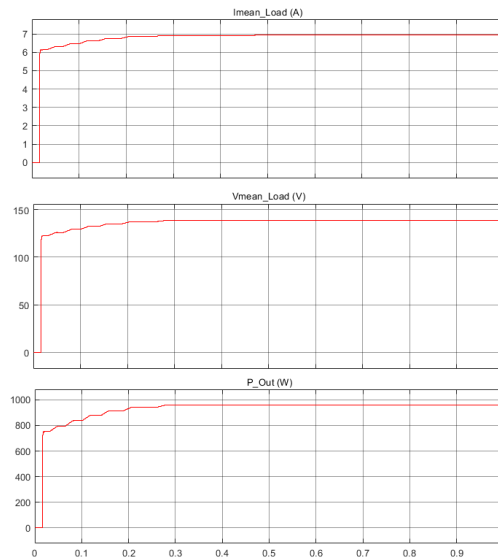


Figure 3.5: Load values without faults.

3.3 No Fault Mode

In this section the first simulation mode will be explained. The first mode is a normal function mode in which no faults occur and the system should work normally. It is expected that the output power will be about 930 W, since each solar panel provides 310 W of power and we have connected 3 modules in series. Also, the MPPT algorithm should be able to quickly find the optimal duty cycle and maintain power production until the end.

The chosen simulation time was 1 second as this should be more than enough time for the system to operate at its optimal point. To show how the system works, the mode "0" and a load of 20Ω were chosen.

As can be seen in the figures 3.4 and 3.5, the system operates normally. The duty cycle stabilises at 0.2, and the load output is about 930 W, with a few losses along the way. To simulate some of the losses, some small resistors were connected in series with the inductor and the capacitors. The final values of some of the measurements are presented in Figure 3.6.

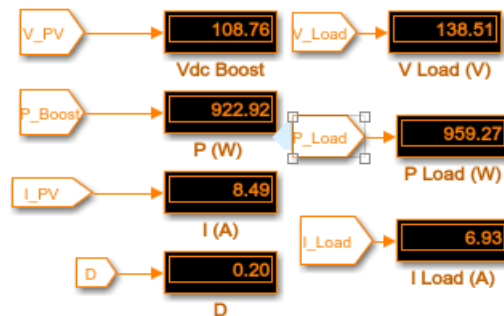


Figure 3.6: Final values after 1 second of simulation.

3.4 Cable Fault

One of the faults to be investigated in this project was a fault in the PV cable. Normally the cable has to be replaced in such a case, as in this study the complete breakage of the cable was simulated. A fault in the cable can occur for various reasons.

The ageing of the cable could be one of the reasons, as its expected lifetime can be greatly reduced if it has worked outside of normal operating conditions. This can lead to embrittlement, cracking and eventually complete failure of the insulating and sheathing materials, resulting in a short circuit and eventual electrical failure. [19]

If the cable has been incorrectly selected for its application, it is also likely to fail in service, and its degradation, moisture, overheating or electrical overload are all possible causes of cable failure. Also, rodent attacks must be avoided as they often attack the outer layers of the cables, resulting in reduced sheathing or insulation and another possible electrical fire. [19]

In order to emulate the breakage of the cable, a switch is connected in series. It has an internal resistance of 0.001Ω and is closed in its initial state. The switch has a gate that is controlled by the MATLAB script and opens at the time of the fault when "Mode 1", i.e. the cable fault, is selected.

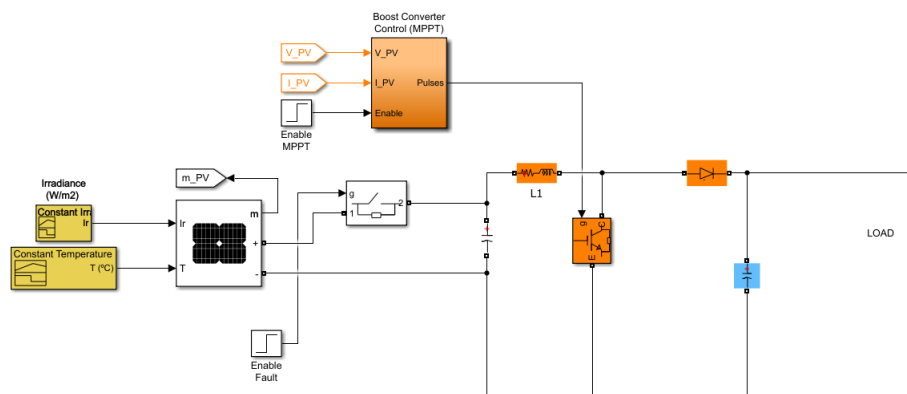


Figure 3.7: Implementation of the cable fault in Simulink.

Once again, the simulation was run with a load of 20Ω , having selected Mode 1. As expected, the load values all drop to 0 after the cable breaks, as it no longer supplies the load. The graphics of all load values are shown in Figure 3.8.

In terms of PV values, there is an increase in all variables, while the duty cycle decreases to its minimum threshold of 0.1. This is due to the small capacitor connected to the panel and the small impedance of the switch used to model this fault, as in a real environment all values would drop to 0 due to a cable break. Without these additional components, the simulation would not be possible. This is evidenced by Figures 3.9 where it is possible to see the the evolution of the PV measurements through the full simulation.

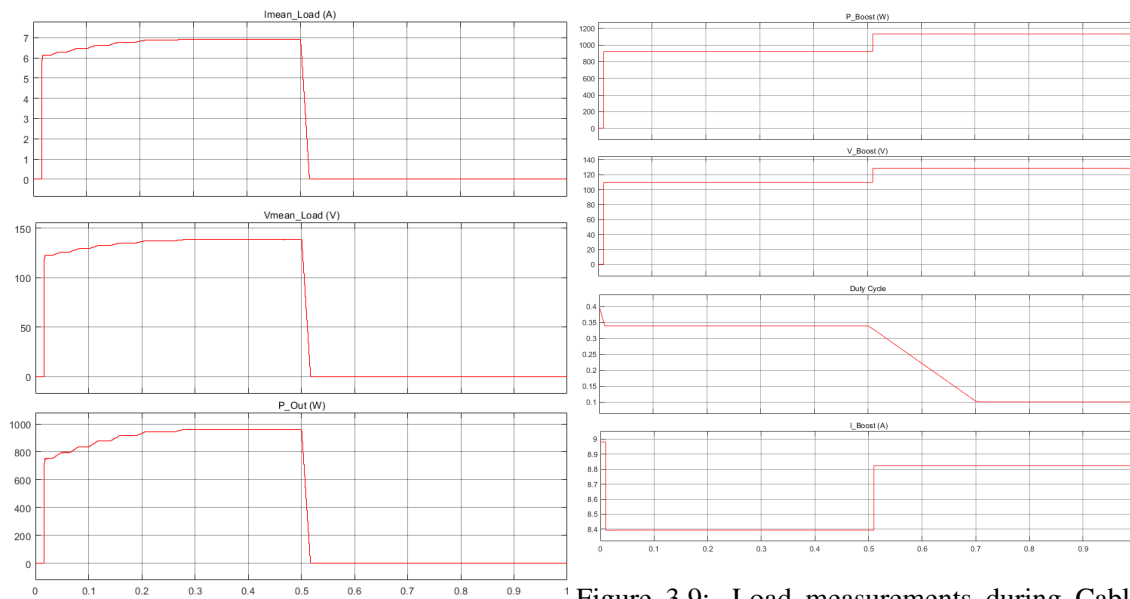


Figure 3.9: Load measurements during Cable fault.

3.5 MPPT Fault

The MPPT algorithm is responsible for improving the efficiency of a PV system by finding the MPP in the non-linear I-V curve of a solar cell. This is also error-prone in real-world environments, since, for example, in the case of partial shading, some parts of the PV module are shaded and a considerable amount of energy is lost as a result, since the shaded module is short-circuited by its bypass diode. Due to the complex multi-peak shape of the P-V curve, traditional algorithms such as the one chosen in this project (Incremental Conductance) cannot work and become invalid. [20]

In order to simulate the occurrence of this fault, the MPPT algorithm is deactivated in the chosen fault time when "Mode 2" is selected. To visualise this event, the load was kept at 20Ω and the fault was introduced at 0.5 seconds.

As can be seen in the figures 3.10 and 3.11, the duty cycle goes back to the default value of 0.4 and all load measurements decrease since the operating point of the I-V curve is not in its optimal value.

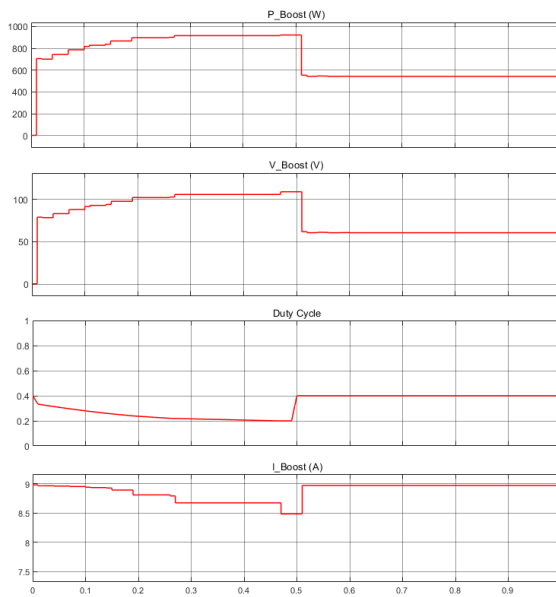


Figure 3.10: PV measurements during MPPT fault.

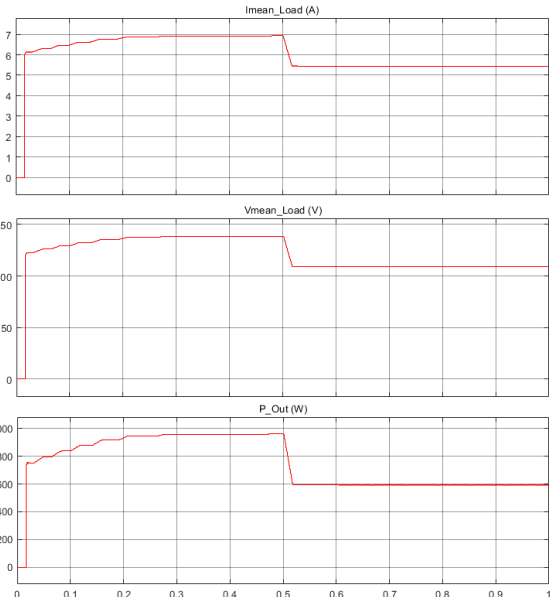


Figure 3.11: Load measurements during MPPT fault.

3.6 SC gate Fault

The gate of the power switch present in DC-DC converters is one of the components that fail most frequently. This can be of two types: SC or OC faults. First, we will take a look at SC faults.

These can occur for a number of reasons. Due to reduced load impedance, faulty driver pulses for the switches or even human error, overcurrents can occur resulting in a SC fault. Parasitic oscillations in the gate, supply voltage errors in the driver stage can lead to overvoltage or overtemperature on the gate, which can cause a SC and consequently a fault. [21]

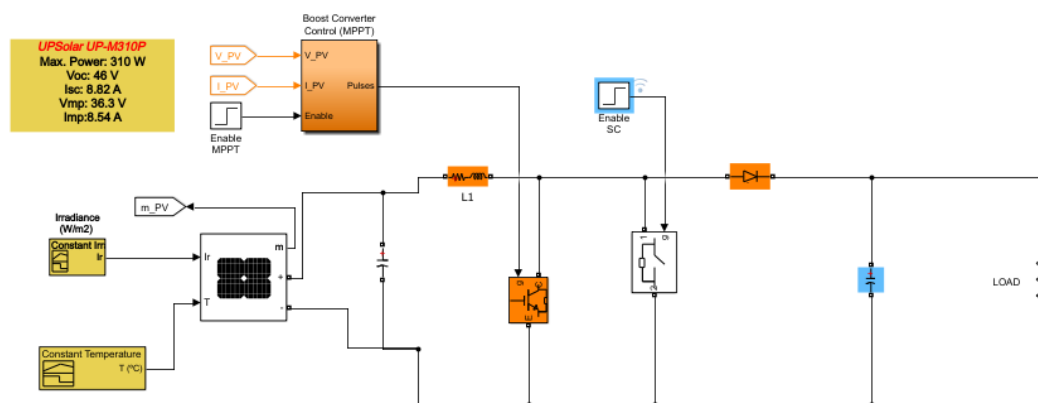


Figure 3.12: Modeled SC Fault in Simulink.

In order to emulate this type of fault, a cable was connected in parallel with the gate. As can

be seen in Figure 3.12, this cable has a switch that is open by default and only close when mode 3 is selected in the MATLAB initialisation script. When this happens, the system behaves as desired as if a short circuit had occurred in the gate.

The same procedure was used to analyse the behaviour of the system: the chosen load was 20Ω , mode 3 was chosen and the fault was introduced at 0.5 seconds. However, this time the simulation was run through 3 seconds. Figures 3.13 and 3.14 show the evolution of the values measured in the converter and in the load. As expected, when a short circuit occurs, no current flows through the load and consequently both voltage and power go to 0. In the converter, the current increases slightly while the voltage fluctuates between 10 and -10V, and slowly converges to 0 over time. In a real scenario, this would not be the behaviour of the circuit, as there would be a spike immediately after the short circuit and afterwards the values would go to 0.

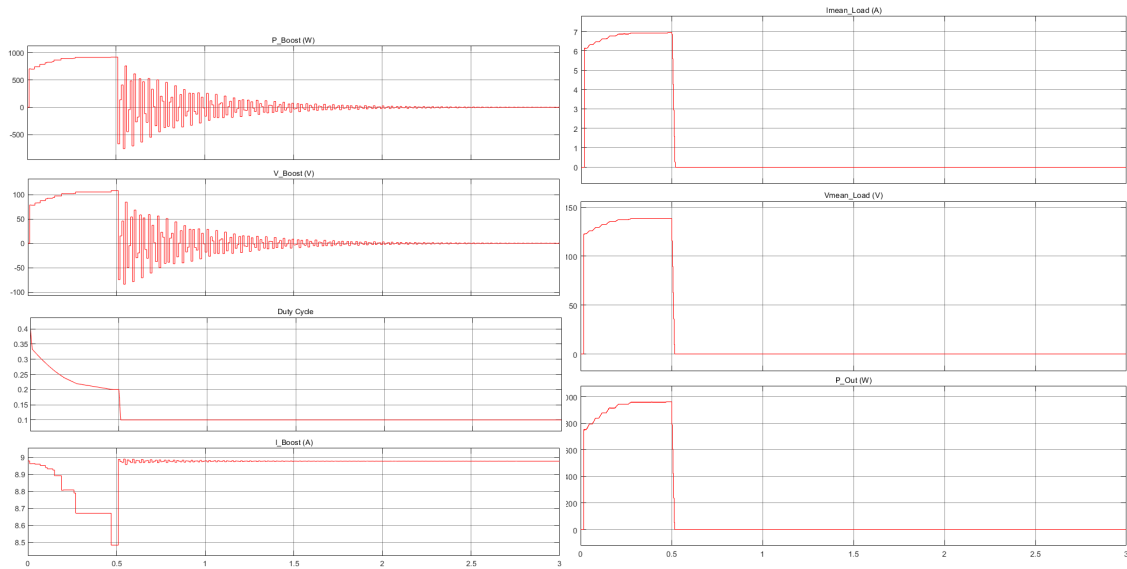


Figure 3.13: PV measurements during SC fault. Figure 3.14: Load measurements during SC fault.

3.7 OC gate Fault

Open-circuit faults in the gate of the transistor are closely related to SC faults, which means that they are usually a consequence of the occurrence of a SC fault. These two types of faults are the most common faults in DC-DC converters and occur mainly due to incorrect gate voltage, driver failure or rupture of the switch. [22]

The topology chosen to emulate the occurrence of a OC fault in the gate of the transistor, a switch was connected in series with the former. This switch is closed by default and is opened when mode 4 is selected in the MATLAB initialisation script. Figure 3.15 shows the modelling of this fault.

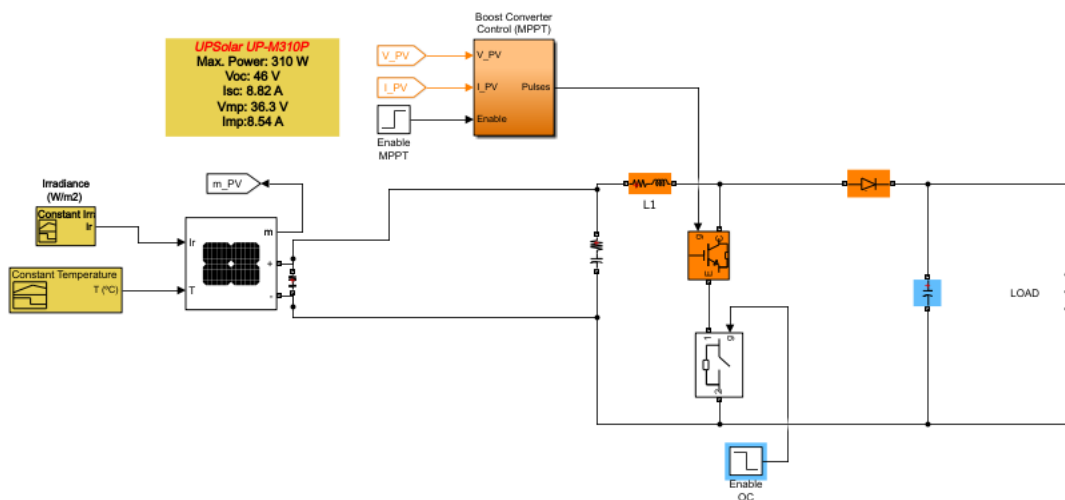


Figure 3.15: Modeled OC Fault in Simulink.

As it was done for every other fault, the load was held at 20Ω , the fault was introduced at 0.5 seconds and the simulation time was 1 second.

Looking at the graphical evolution of the measurements in the converter, it is easy to see the behaviour of the circuit. The voltage increases slightly and both the current and the power decrease. The duty cycle increases until it reaches the threshold value of 0.9. In the load, each measured value decreases. The graphics can be seen in figures 3.16 and 3.17.

3.8 Intermittence Fault

The last fault chosen to be investigated in this project is an intermittence fault. This can happen when the connections are poorly made and the signals sent by the MPPT control are not being sent continuously.

To visualise this effect, a fault was inserted at 0.5 seconds. In Figure 3.18 it is possible to see the effect of this fault as a graph is shown between 0.49 and 0.5015 seconds. The first graph is the signal sent by the MPPT algorithm. As can be seen from the output signal going to the converter, it is slightly adjusted as an intermittence fault occurred and is affecting the final result. Similar

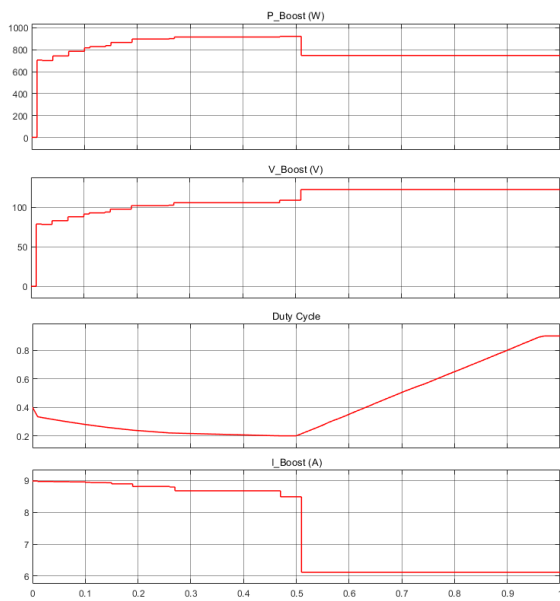


Figure 3.16: PV measurements during OC fault.

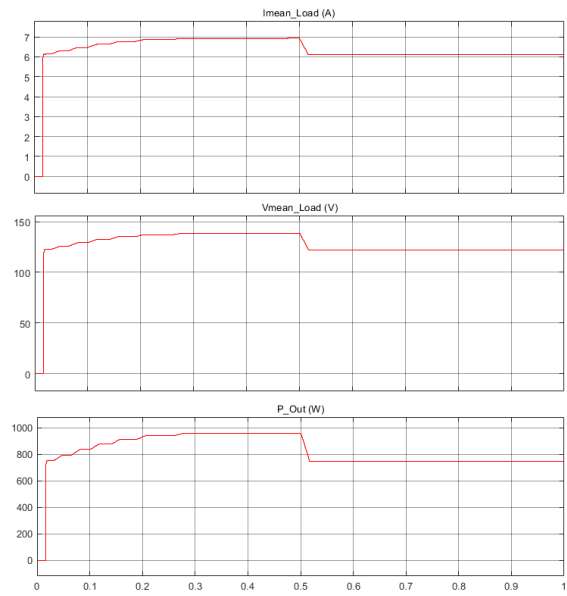


Figure 3.17: Load measurements during OC fault.

to the MPPT fault, which is another type of error in this system as it is unable to properly do its function, load current, voltage and power decrease as can be seen in Figure 3.19.

While the current increases, both voltage and current in the converter decrease, and in the latter it is possible to see the effect of the intermittence, since they do not remain constant, floating until the end of the simulation.



Figure 3.18: Influence of intermittence fault.

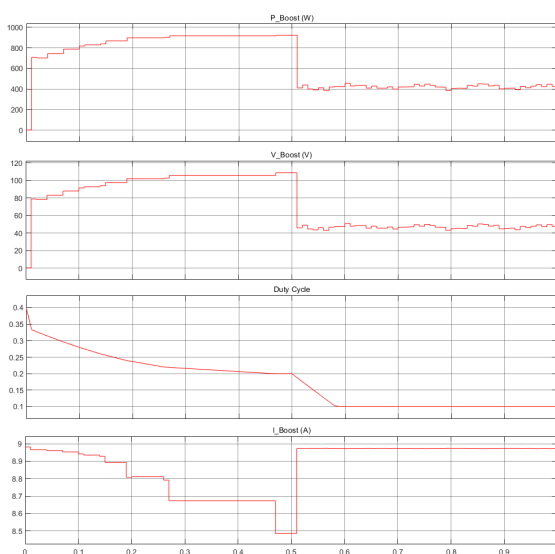


Figure 3.19: PV measurements during fault.

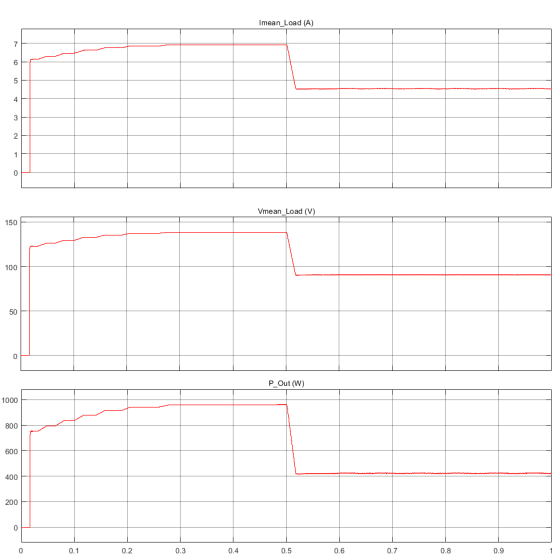


Figure 3.20: Load measurements during fault.

Chapter 4

Fault Diagnosis Algorithms

This chapter discusses the proposed approaches for fault detection in DC-DC converters used in PV systems. Different methods have been applied, starting with a signal-based algorithm without a digital twin and then 3 different approaches using the DT.

4.1 Signal-Based Algorithm

Taking into account the previously defined faults, it was intended to design an algorithm that should be developed that is able to detect the occurrence of the same faults without the digital twin. The approach taken in this algorithm was by the mean of analysis of a considerable number of variables and compare the values obtained with a unit delay of 2 time steps, as shown in Figure 4.1.

Some of the variables selected for investigation are not commonly measured in a real/commercial environment, but are necessary for the proper functioning of the algorithm. Further in this project it was investigated whether the system could maintain its effectiveness without these specific variables.

In particular, the OC/SC current and voltage are problematic as they are not easy to measure as they generally do not have accessible terminals and therefore were avoided to be chosen as diagnostic variables. Figure 4.2 shows the specific locations of these measurements, highlighted in blue.

To gain a broader perspective on the behaviour of the circuit, several variables were assessed. These are summarised in the Table 4.1. For each fault introduced through the MATLAB script, the simulation time and the time of the fault was maintained constant, being 1 second for each of these, having a fault appear at 0.5 seconds. The function "to workspace" was used to transfer the values obtained in Simulink to the MATLAB workspace. In this way, an array with 500 000 units was created for 1 second of simulation.

In this approach, the irradiance and temperature were kept constant and only the values of the load were changed. The variables were compared at 4 different time periods: The entire simulation, during the fault (where only the values after 0.5 seconds were compared), "healthy"

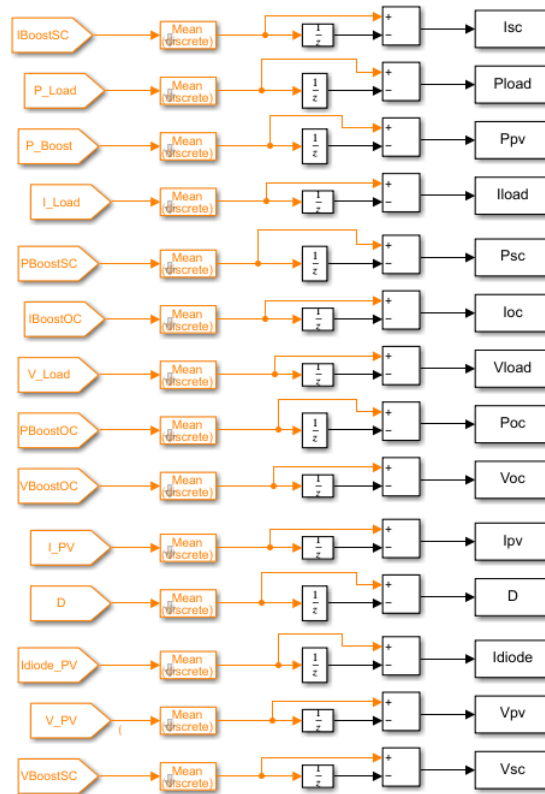


Figure 4.1: Example of the data study.

values (before the fault) and the "transition" values. The last period was considered the most relevant, as the algorithm aims to detect the fault immediately, in order to minimise the problems that each one could bring to the converter and the whole system. This period was considered between 0.502 and 0.517 seconds, as when taking a look at the difference peaks when an error occurs this is where it is most relevant. Table 4.2 shows a summary of these time periods.

At an irradiance of 1000 W/m^2 and a temperature of 25°C , the MPPT algorithm can operate between 17 and 56Ω accurately. Therefore, simulations with loads of 20 , 30 , 40 and 50Ω were performed for each fault.

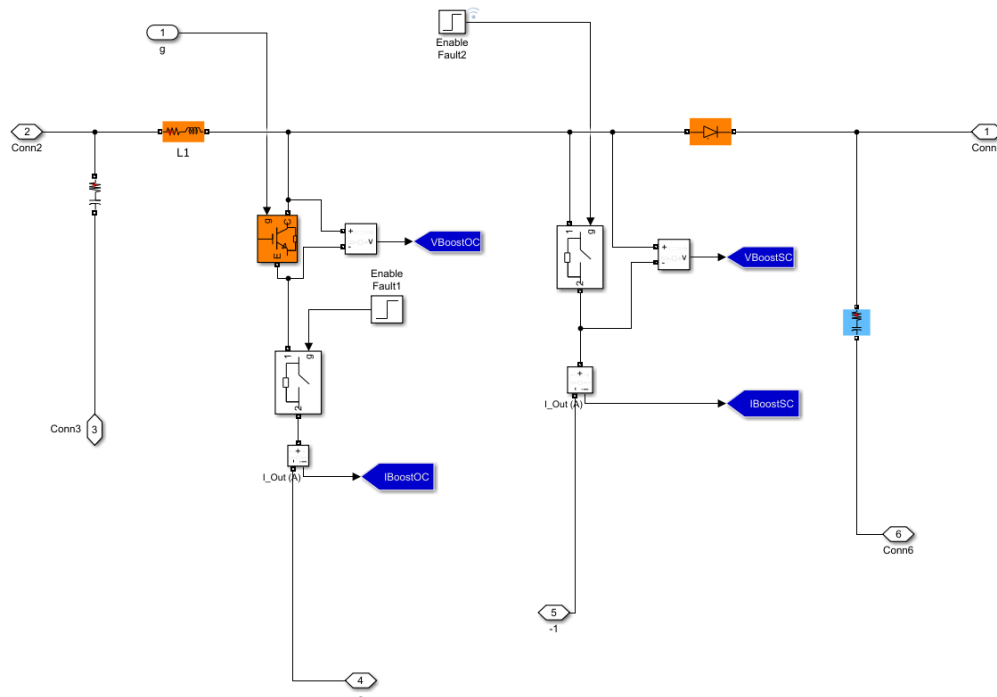


Figure 4.2: Location of OC and SC measurements.

4.1.1 Cable Fault

The first fault to be implemented in the algorithm was a fault in the PV cable. As mentioned earlier, different simulations were performed for this fault, keeping the previously mentioned parameters. The results of the differences in the transition values can be seen in Table 4.3.

Looking at the analysis previously performed for this type of fault, the results are consistent with those previously obtained. The voltage of the converter increases while the voltage and current in the load decrease, for example. The goal of the study is to find characteristics that are reasonably linear and different from the other faults, so that no cable fault warning appears when another type of fault occurs.

For example, the change in P_{PV} is relatively large compared to the other variables, but it decreases significantly at a load of 40Ω , while it increases at any other load. For this reason, this variable was not considered for the algorithm. Therefore, P_{Load} , V_{Load} , V_{PV} and I_{Load} were chosen as diagnostic variables for this algorithm.

A study was carried out to establish a function preferably related to R_{Load} . The obtained formulas can be seen in the Table 4.4. For each load value, there is a small gap between the average value and the selected threshold, i.e., if in a given period the differences of P_{Load} , V_{Load} , V_{PV} and I_{Load} are at least the values in the Table 4.4, it means that a fault must have occurred in the PV cable. In addition, a transient correction was implemented for each algorithm, being this a step up function starting at 0 and increasing to 1 after 0.1 seconds. The purpose of this correction is to ensure that no error is reported due to the transient behaviour at the beginning of the circuit

Table 4.1: Studied variables.

Variables	Units
V_{Load}	V
I_{Load}	A
P_{Load}	W
V_{PV}	V
I_{PV}	A
P_{PV}	W
I_{Diode}	A
V_{OC}	V
I_{OC}	A
P_{OC}	W
V_{SC}	V
I_{SC}	A
P_{SC}	W
Duty Cycle	%

actuation. The implementation of this algorithm in MATLAB Simulink can also be seen in Figure 4.3, where the warning flag was activated when a cable fault was introduced into the system.

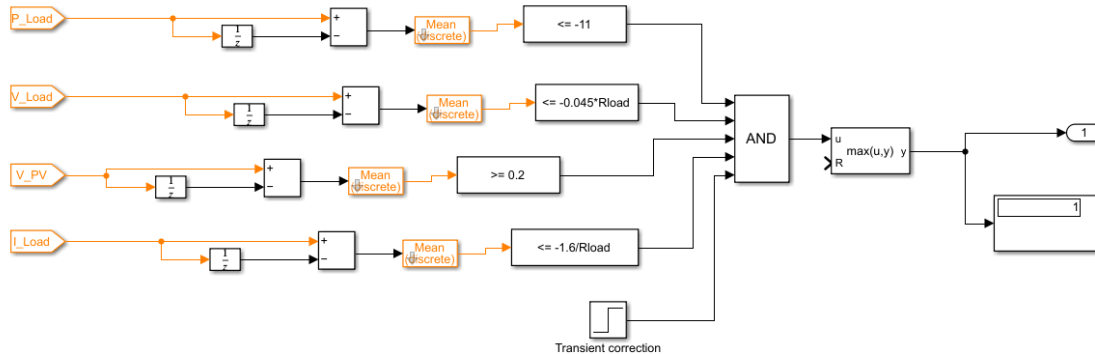


Figure 4.3: Cable fault algorithm in Simulink.

Table 4.2: Chosen time periods.

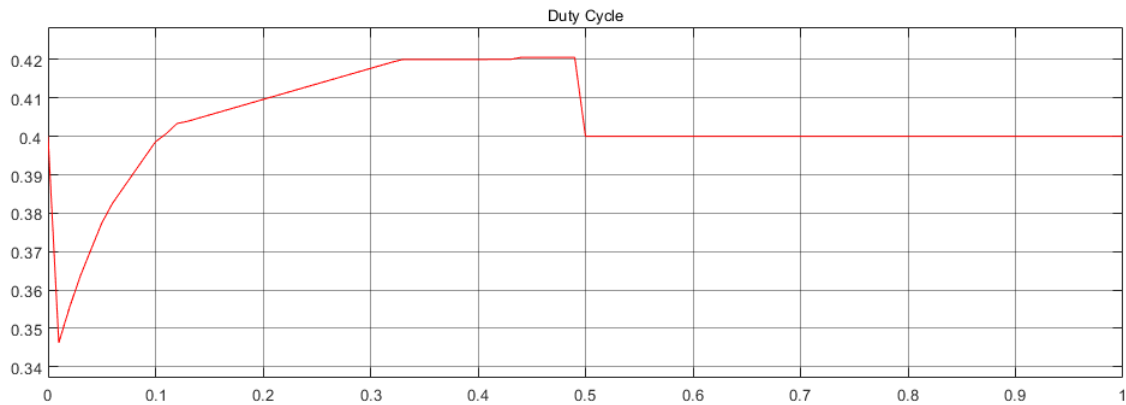
Name	Time period (s)
All	0-1
Healthy	0-0.5
Fault	0.5-1
Transition	0.502-0.517

4.1.2 MPPT Fault

The same data study was conducted for this fault type as for the other faults. In Table 4.5 shows the data obtained during this study.

The algorithm for the MPPT fault followed the premise that since the MPPT is responsible for optimising power generation by reaching the maximum power on the I-V curve, so that when it stops working, every load measurement decreases. This is also an effect seen in Chapter 3.

Clearly there is one issue with this method for which there is a valid reason behind it. If we look at the measurements when the load is 40Ω , the behaviour is definitely different than any other resistor. This is because when the fault occurs, the duty cycle returns to the default value of 0.4, which is also similar to the optimal value obtained for this particular load (0.42, Figure 4.4).

Figure 4.4: Duty cycle evolution with $R_{Load}=40\Omega$ for MPPT fault.

Using this logic, it can be assumed that an MPPT fault occurring at this load value in this project is not actually a fault because it does not affect the output production.

For any other load, an algorithm was developed. The values obtained can be seen in Table 4.6, while its implementation in Simulink and the validation of the warning flag can be seen in Figure 4.5. As with the cable fault a transient correction has been implemented, as well as a condition where the duty cycle is equal to the default value of 0.4.

4.1.3 SC Fault

The same analysis is performed to investigate the SC fault. Maintaining an irradiance of $1000W/m^2$ and a temperature of $25\text{ }^\circ\text{C}$, the load was increased from $20\ \Omega$ to $50\ \Omega$ and the diagnostic variables

Table 4.3: Simulation results for Cable fault.

Load(Ω)	Transition_D	Transition_ I_{Diode}	Transition_ I_{Load}	Transition_ I_{OC}
20	-1.14E-04	0.25467413	-0.08304587	-1.97E-05
30	-1.15E-04	0.253579498	-0.067680741	-2.29E-05
40	0.002846837	-0.050135299	-0.058138336	-2.63E-05
50	-1.15E-04	0.255138681	-0.051393719	-2.83E-05

Load(Ω)	Transition_ I_{PV}	Transition_ I_{SC}	Transition_ P_{Load}	Transition_ P_{OC}
20	0.051120936	-1.97E-05	-11.53108329	-0.002226577
30	0.052210728	-2.29E-05	-11.59035126	-0.003427949
40	-0.255710561	-2.63E-05	-11.55704907	-0.004566351
50	0.050647497	-2.83E-05	-11.47407491	-0.005723849

Load(Ω)	Transition_ P_{PV}	Transition_ P_{SC}	Transition_ V_{Load}	Transition_ V_{OC}
20	8.568899394	-0.002226577	-1.660917406	-1.972967651
30	8.575215832	-0.003427949	-2.030422225	-2.289732522
40	-30.69993002	-0.004566348	-2.32553346	-2.633064452
50	8.594573708	-0.005723855	-2.569685949	-2.825668132

Load(Ω)	Transition_ V_{PV}	Transition_ V_{SC}
20	0.236126474	-1.972967659
30	0.222756792	-2.289732545
40	0.249792738	-2.633064484
50	0.244879912	-2.82566816

Table 4.4: Cable fault Signal-Based algorithm

Diagnostic Variable	Load (Ω)	Measured Values	Condition	Condition Value
I_{Load}	20	-0.08304587	$< -1,6/R_{Load}$	0.08
	30	-0.067680741		0.053333333
	40	-0.058138336		0.04
	50	-0.051393719		0.032
V_{Load}	20	-1.660917406	$< -R_{Load} * 0.045$	0.9
	30	-2.030422225		1.35
	40	-2.32553346		1.8
	50	-2.569685949		2.25
P_{Load}	20	-11.53108329	< -11	-11
	30	-11.59035126		-11
	40	-11.55704907		-11
	50	-11.47407491		-11
V_{PV}	20	0.236126474	> 0.2	0.2
	30	0.222756792		0.2
	40	0.249792738		0.2
	50	0.244879912		0.2

Table 4.5: MPPT fault simulation results.

Load (Ω)	Transition_D	Transition_ I_{Diode}	Transition_ I_{Load}	Transition_ V_{OC}
20	0.002385364	-0.005747183	-0.016617203	-0.019978611
30	0.000726982	-0.006562432	-0.00294476	-0.019946406
40	-0.000238447	0.004013457	0.00037712	-0.018367659
50	-0.000956226	0.018822116	-0.002375336	-0.015681093

Load (Ω)	Transition_ I_{PV}	Transition_ I_{SC}	Transition_ P_{Load}	Transition_ P_{OC}
20	0.005821412	-1.00451E-06	-4.151176016	-0.000768077
30	0.006578153	2.59566E-06	-0.987483062	6.79528E-05
40	-0.003997287	4.42119E-06	0.144223013	0.000723617
50	-0.018771057	3.36295E-06	-1.019655571	0.000307871

Load (Ω)	Transition_ P_{PV}	Transition_ P_{SC}	Transition_ V_{Load}	Transition_ V_{OC}
20	-4.510051565	-0.000588831	-0.332344059	-0.100431506
30	-1.297300309	0.000246417	-0.088342796	0.259586104
40	-0.043038312	0.000875044	0.015084803	0.442137036
50	-1.047741395	0.000418253	-0.118766804	0.336310954

Load (Ω)	Transition_ V_{PV}	Transition_ V_{SC}
20	-0.573368266	-0.100451483
30	-0.225891769	0.25956616
40	0.047015554	0.442118672
50	0.137912748	0.336295272

Table 4.6: MPPT fault Signal-Based algorithm

Diagnostic Variable	Load (Ω)	Measured Values	Condition	Condition Value
V_{Load}	20	-0.332344059	< -0.11	-0.11
	30	-0.088342796		-0.11
	40	0.015084803		-0.11
	50	-0.118766804		-0.11
I_{Load}	20	-0.016617203	< $0.1/R_{Load}$	-0.005
	30	-0.00294476		-0.003333333
	40	0.00037712		-0.0025
	50	-0.002375336		-0.002
P_{Load}	20	-4.151176016	< $20/R_{Load}$	-1
	30	-0.987483062		-0.666666667
	40	0.144223013		-0.5
	50	-1.019655571		-0.4

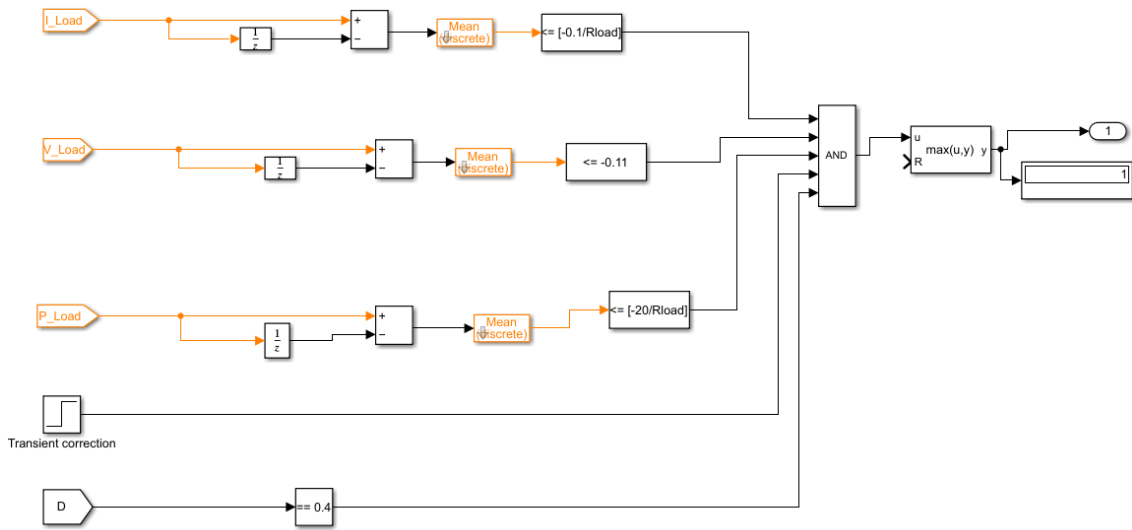


Figure 4.5: MPPT fault algorithm in Simulink.

from Table 4.1 were analysed. Table 4.7 shows the data obtained by this study.

Following the same logic as before, P_{Boost} , P_{Load} , V_{Load} , $V_{BoostOC}$, and $V_{BoostSC}$ were selected as diagnostic variables. These variables evolved reasonably linearly and showed a significant difference with the occurrence of a fault. After studying the evolution of these variables, the algorithm was defined as seen in Table 4.8.

The implementation of this algorithm in Simulink can also be seen in Figure 4.6, having the positive warning as this was the fault introduced with a load of 23Ω in the MATLAB script.

4.1.4 OC Fault

As with the previous faults, the data study remained the same: the variables mentioned in the Table 4.1 were analysed in the transition period for different loads and evaluated whether they were relevant to the algorithm or not, with the results obtained exposed in Table 4.9.

In particular, this algorithm was quite difficult to create because the changes in diagnostic variables were quite similar to some of the other algorithms. For this reason, several variables were selected as diagnostic variables, as can be seen in Table 4.10.

Some of the diagnostic variables chosen in this algorithm are the same as those chosen for other types of fault. Especially P_{Load} and $V_{BoostSC}$ can be problematic because they behave similarly for cable and SC faults, respectively. For a cable fault, P_{Load} always decreases around 11 W on average, while for OC faults the value is at most 7.6 W at higher loads. To prevent a false positive OC fault warning from being issued when a cable fault occurs, a threshold of 8 W has been set, i.e. if the decrease in P_{Load} is higher than 8 W, no OC fault can have occurred. The same logic was applied to $V_{BoostSC}$ with respect to the SC fault. This threshold was defined as a maximum decrease of 1.15 V for a OC fault.

Table 4.7: SC fault simulation results.

Load(Ω)	Transition_D	Transition I_{Diode}	Transition P_{Load}	Transition P_{OC}
20	-0.001198629	-0.005559684	-11.531492	-0.002315027
30	-0.002868139	-0.006636888	-11.59357187	-0.003487359
40	-0.003840047	-0.004601326	-11.56621285	-0.004638504
50	-0.004562638	-0.004425786	-11.49978418	-0.005769455

Load(Ω)	Transition P_{PV}	Transition P_{SC}	Transition V_{Load}	Transition V_{OC}
20	-11.25341165	-7.78E-04	-1.662324029	-1.663505106
30	-11.25232224	-0.001945418	-2.03543892	-2.043018155
40	-11.24109093	-0.003106576	-2.335268388	-2.356966323
50	-11.23643028	-0.004238447	-2.58525938	-2.629143028

Load(Ω)	Transition V_{PV}	Transition V_{SC}	Transition I_{Load}	Transition V_{OC}
20	-1.32197351	-1.66350699	-0.083116201	-0.0018849
30	-1.335682136	-2.043020045	-0.067847964	-0.001889516
40	-1.308248528	-2.356968215	-0.05838171	-0.001891236
50	-1.30548078	-2.629144921	-0.051705188	-0.001893859

Load(Ω)	Transition I_{PV}	Transition I_{SC}
20	0.005743872	0.108048137
30	0.006814355	0.108043382
40	0.00477676	0.1081119
50	0.004599498	0.108125374

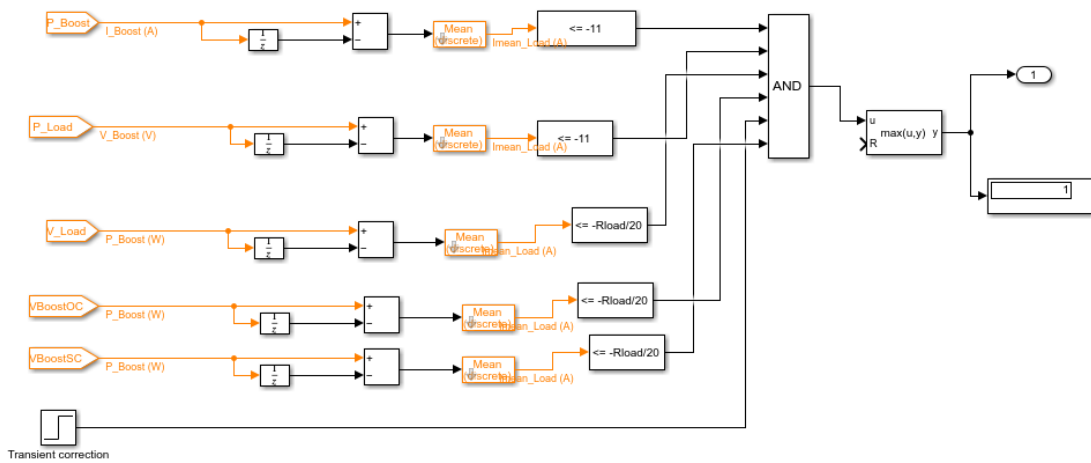


Figure 4.6: SC fault algorithm in Simulink.

Table 4.8: SC fault Signal-Based algorithm.

Diagnostic Variable	Load (Ω)	Measured Values	Condition	Condition Value
P_{Load}	20	-11.531492	< -11	-11
	30	-11.59357187		-11
	40	-11.56621285		-11
	50	-11.49978418		-11
P_{PV}	20	-11.25341165	< -11	-11
	30	-11.25232224		-11
	40	-11.24109093		-11
	50	-11.23643028		-11
V_{Load}	20	-1.662324029	$< -R_{Load}/20$	-1
	30	-2.03543892		-1.5
	40	-2.335268388		-2
	50	-2.58525938		-2.5
V_{oc}	20	-1.663505106	$< -R_{Load}/20$	-1
	30	-2.043018155		-1.5
	40	-2.356966323		-2
	50	-2.629143028		-2.5
VSC	20	-1.66350699	$< -R_{Load}/20$	-1
	30	-2.043020045		-1.5
	40	-2.356968215		-2
	50	-2.629144921		-2.5

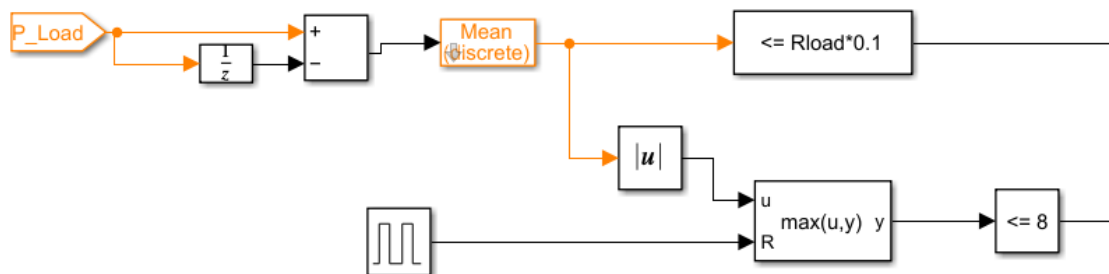


Figure 4.7: Implementation of a maximum threshold.

Table 4.9: OC fault simulation results.

Load (Ω)	Transition_D	Transition_ I_{Diode}	Transition_ I_{Load}	Transition_ V_{OC}
20	1.60E-04	0.028324866	-0.009767109	-1.00E-05
30	0.00287941	-0.011847782	-0.017701982	-1.49E-05
40	-4.18E-04	0.152789237	-0.020837028	-1.73E-05
50	-2.87E-04	0.174293367	-0.022065124	-2.02E-05

Load (Ω)	Transition_ I_{PV}	Transition_ I_{SC}	Transition_ P_{Load}	Transition_ P_{OC}
20	-0.028350979	-1.95E-06	-2.549061814	-0.001812427
30	-0.112079933	-5.31E-06	-5.243022866	-0.002875855
40	0.024036973	-8.33E-06	-6.733567335	-0.004060949
50	0.030310088	-1.10E-05	-7.635954109	-0.00517443

Load (Ω)	Transition_ P_{PV}	Transition_ P_{SC}	Transition_ V_{Load}	Transition_ V_{OC}
20	-2.087468499	-5.10E-04	-0.195342182	-0.856252832
30	-12.49741346	-0.001572927	-0.531059447	-1.08643905
40	4.982998279	-0.002693455	-0.833481101	-1.461865278
50	5.858727014	-0.003818012	-1.10325618	-1.70836821

Load (Ω)	Transition_ V_{PV}	Transition_ V_{SC}
20	0.162730195	-0.195344759
30	0.190676237	-0.531064021
40	0.226601811	-0.833486988
50	0.234369124	-1.103262755

Table 4.10: OC fault signal-based algorithm.

Diagnostic Variable	Load (Ω)	Measured Values	Condition	Condition Values
V_{Load}	20	-0.195342182	$< R_{Load} * -0.008$	-0.16
	30	-0.531059447		-0.24
	40	-0.833481101		-0.32
	50	-1.10325618		-0.4
V_{OC}	20	-0.856252832	$< R_{Load} * -0.03$	-0.6
	30	-1.08643905		-0.9
	40	-1.461865278		-1.2
	50	-1.70836821		-1.5
V_{PV}	20	0.162730195	$< R_{Load} * 0.0045$	0.09
	30	0.190676237		0.135
	40	0.226601811		0.18
	50	0.234369124		0.225
VSC	20	-0.195344759	$< R_{Load} * -0.008$	-0.16
	30	-0.531064021		-0.24
	40	-0.833486988		-0.32
	50	-1.103262755		-0.4
I_{OC}	20	-1.00274E-05	$< R_{Load} * -4E - 7$	-8.00E-06
	30	-1.48775E-05		-1.20E-05
	40	-1.7287E-05		-1.60E-05
	50	-2.02415E-05		-2.00E-05

The blocks shown in Figure 4.7 illustrate this implementation. The MinMax Running Resettable block maintains the maximum value reached until it is reset. The input for this block is the module of the comparison between the instantaneous value and the delayed value.

A pulse generator with a period of 0.4 seconds controls the reset operation to ignore a possible maximum value above the threshold for the initial transient behaviour of the circuit.

A condition was then set where the output of the MinMax Running Resettable is less than the defined threshold, having the logic correctly implemented in the system. In Figure 4.8 the full implementation of the algorithm is shown.

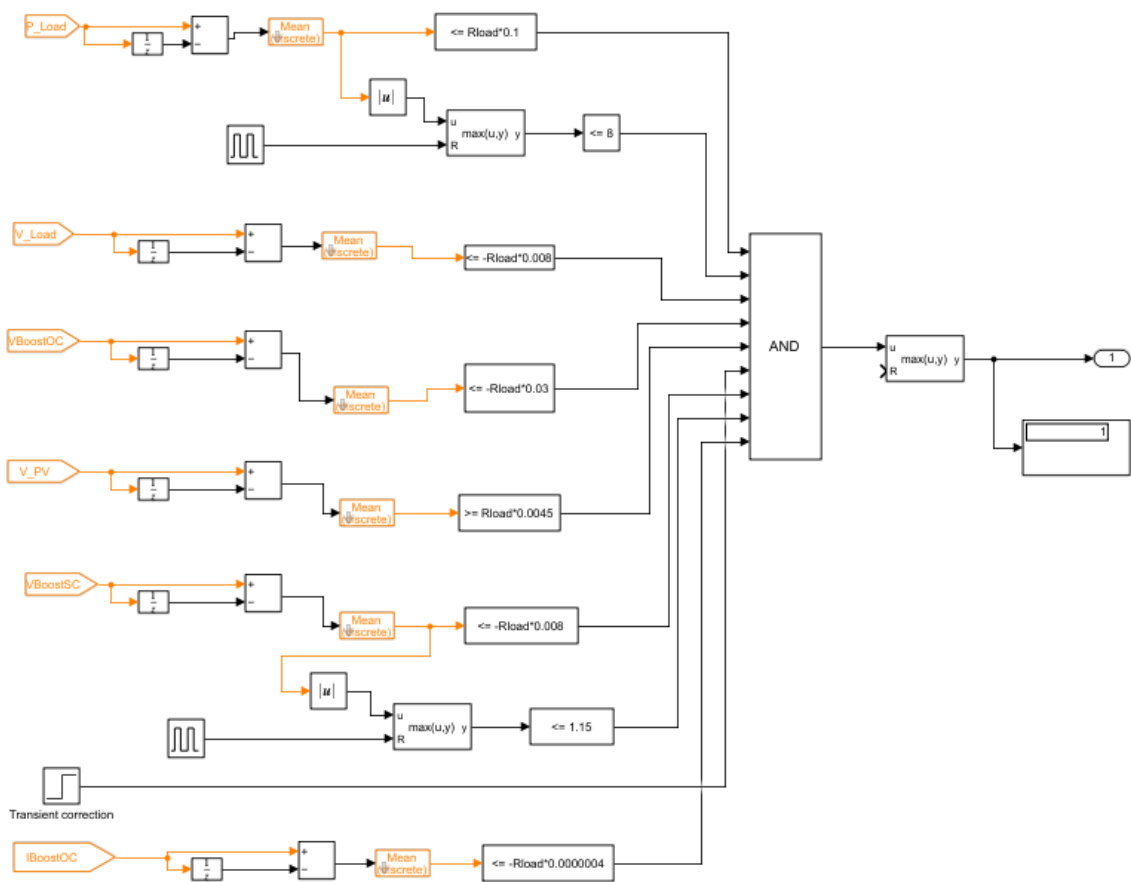


Figure 4.8: OC fault algorithm in Simulink.

Table 4.11: Intermittence fault simulation results.

Load(Ω)	Transition_D	Transition_ I_{Diode}	Transition_ I_{Load}	Transition_ V_{OC}
20	-1.37E-04	-0.005748607	-0.029274707	5.65E-02
30	-7.92E-05	-0.006837973	-0.014116715	5.85E-02
40	-5.08E-05	-0.004533565	-0.005199879	5.99E-02
50	-4.70E-06	2.30E-05	-0.001254642	5.87E-02

Load(Ω)	Transition_ I_{PV}	Transition_ I_{SC}	Transition_ P_{Load}	Transition_ P_{OC}
20	0.00584894	-1.12E-05	-6.561878329	-1.27E-03
30	0.006893439	-1.24E-05	-4.260662463	-1.79E-03
40	0.004548442	-1.30E-05	-1.930893099	-2.10E-03
50	-4.08E-05	-1.38E-05	-0.533240435	-2.47E-03

Load(Ω)	Transition_ P_{PV}	Transition_ P_{SC}	Transition_ V_{Load}	Transition_ V_{OC}
20	-6.10477801	-1.77E-03	-0.585494132	-1.119972964
30	-3.77453827	-0.00233263	-0.423501459	-1.240171936
40	-1.44049659	-2.66E-03	-0.207995171	-1.302787716
50	-0.02867599	-0.003008333	-0.062732109	-1.382185451

Load(Ω)	Transition_ V_{PV}	Transition_ V_{SC}
20	-0.751284387	-1.119916511
30	-0.505303065	-1.240113405
40	-0.215691517	-1.302727842
50	-0.002552797	-1.382126762

4.1.5 Intermittence fault

The Intermittence fault is the last fault implemented and went through the same procedure as the others. The results of the data study performed for this fault can be seen in Table 4.11.

The behaviour of this fault is such that an algorithm was not so easy to develop. If we take a look at almost all variables, the behaviour for the load evolution is far from linear. For example, analysing the difference values for P_{PV} , it starts at a rate of -6.10 W at $R_{Load} = 20\Omega$, one of the highest changes across all variables, while at $R_{Load} = 50\Omega$ it only decreases by -0.029 W, a non-significant value. Almost every relevant value exhibits this behaviour, and for this reason the algorithm does not work perfectly at higher loads.

However, when the load is higher, the loss in production is not significant when compared to lower loads, so in a real scenario and since this type of fault is usually due to poor connections and does not affect the health of the system, the fact that the algorithm cannot detect the fault is not considered a major problem.

The study was performed and the obtained algorithm is shown in Table 4.12. As with the OC fault, a maximum threshold was set for some variables: A maximum rate of -8 W for P_{Load} , and a maximum of -0.7 V for V_{Load} . The implementation of the algorithm in Simulink is shown in Figure 4.9.

Table 4.12: Intermittence fault Signal-Based algorithm.

Diagnostic Variable	Load (Ω)	Measured Values	Condition	Condition Values
P_{Load}	20	-6.561878329	$< -75/R_{Load}$	-3.75
	30	-4.260662463	AND	-2.5
	40	-4.260662463		-1.875
	50	-0.533240435	$Max P_{Load} < 8$	-1.5
P_{PV}	20	-6.10477801	$< 50/-R_{Load}$	-2.5
	30	-3.77453827		-1.666666667
	40	-3.77453827		-1.25
	50	-0.02867599		-1
V_{Load}	20	-0.585494132	$< (8/-R_{Load})$	-0.4
	30	-0.423501459	AND	-0.266666667
	40	-0.423501459		-0.2
	50	-0.062732109	$Max V_{Load} < 0.7$	-0.16
V_{OC}	20	-1.119972964	< -1	-1
	30	-1.240171936		-1
	40	-1.240171936		-1
	50	-1.382185451		-1
vsc	20	-1.119916511	< -1	-1
	30	-1.240113405		-1
	40	-1.240113405		-1
	50	-1.382126762		-1
V_{PV}	20	-0.751284387	$< 8/-R_{Load}$	-0.4
	30	-0.505303065		-0.266666667
	40	-0.215691517		-0.2
	50	-0.002552797		-0.16

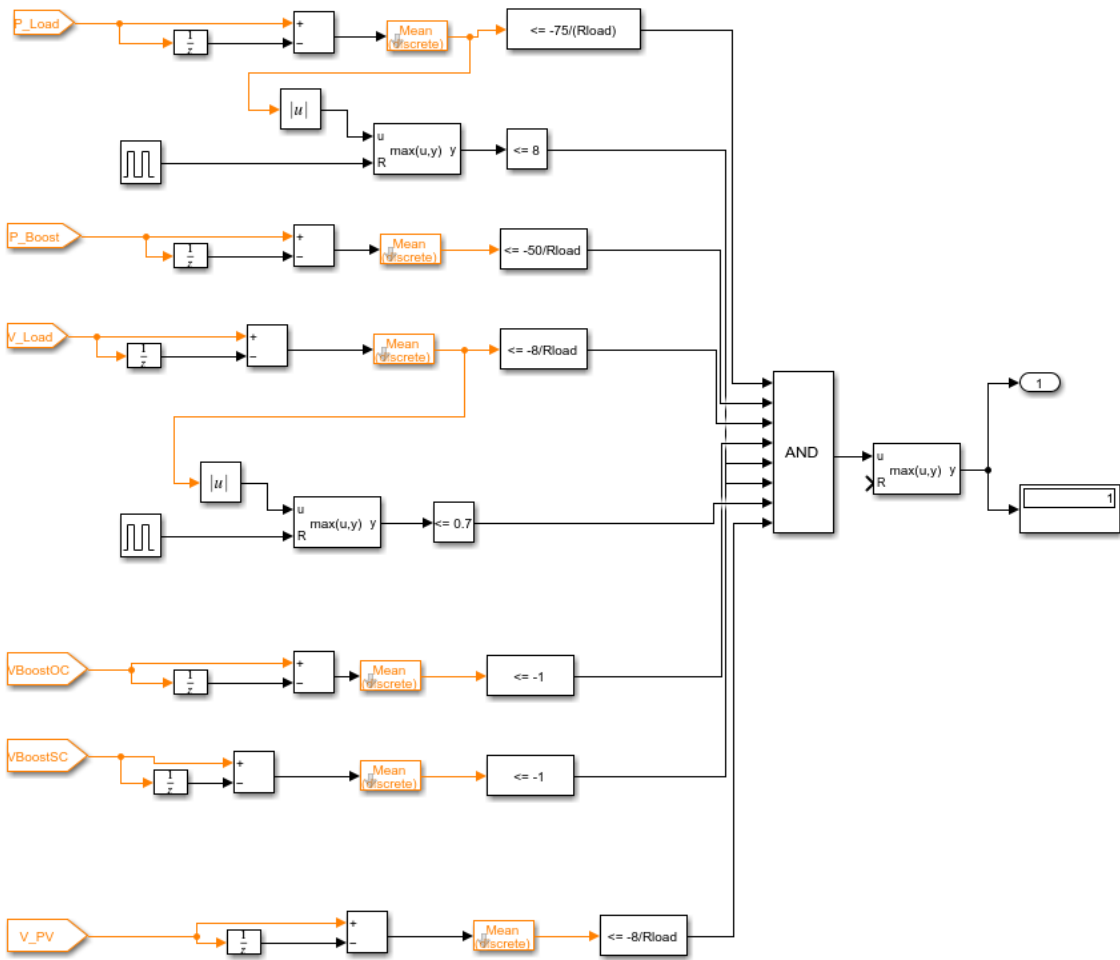


Figure 4.9: Implementation of the algorithm in Simulink.

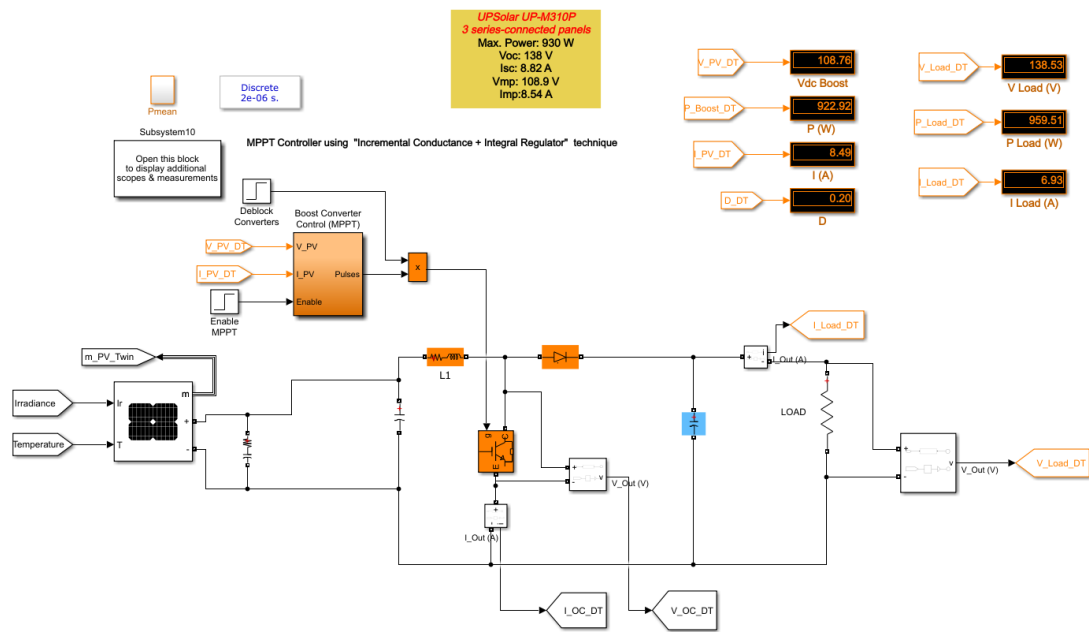


Figure 4.10: Digital Twin in Simulink.

4.2 Digital Twin

This subsection explains the logic behind the Digital Twin. Its goal is to emulate a physical system in order to achieve higher reliability, availability, and maintainability at lower cost. [23] The definition of DT is still volatile as it is a novel technology, especially when applied to power electronics, as explained previously in section 2.

In the case of this project, no physical system was available, so some changes were made to the concept. The supposed "physical twin" in this case was the PV system previously explained and used in this project, and a new DC-DC converter simulation was created as a digital twin, as seen in Figure 4.10.

The digital twin, unlike the previous PV system, does not have any modelled faults, as it is intended to function properly and serves as a benchmark to its physical twin. To emulate the delay between a physical system and a digital simulation, the control time step was doubled to emulate a delay of the data acquisition and in this case is 2μ seconds.

The goal of this DT is to detect and identify the occurrence of the same faults previously explained. Different simulations were performed, but this time the method of data collection was not the same. As can be seen in Figure 4.11, a comparison was made between the PV system and its digital twin, collecting the same variables as in Table 4.1, except for the "SC" measurements. Since it is not necessary to emulate faults in the DT, there is no additional cable in parallel with the transistor, so no measurements were made in this element.

The same MATLAB script was used, as well as the same simulation time periods being the "transition" one (between 0.502 and 0.517 seconds) being the most relevant, as all faults were introduced at 0.5 seconds in this study and as previously studied is the period where the variables

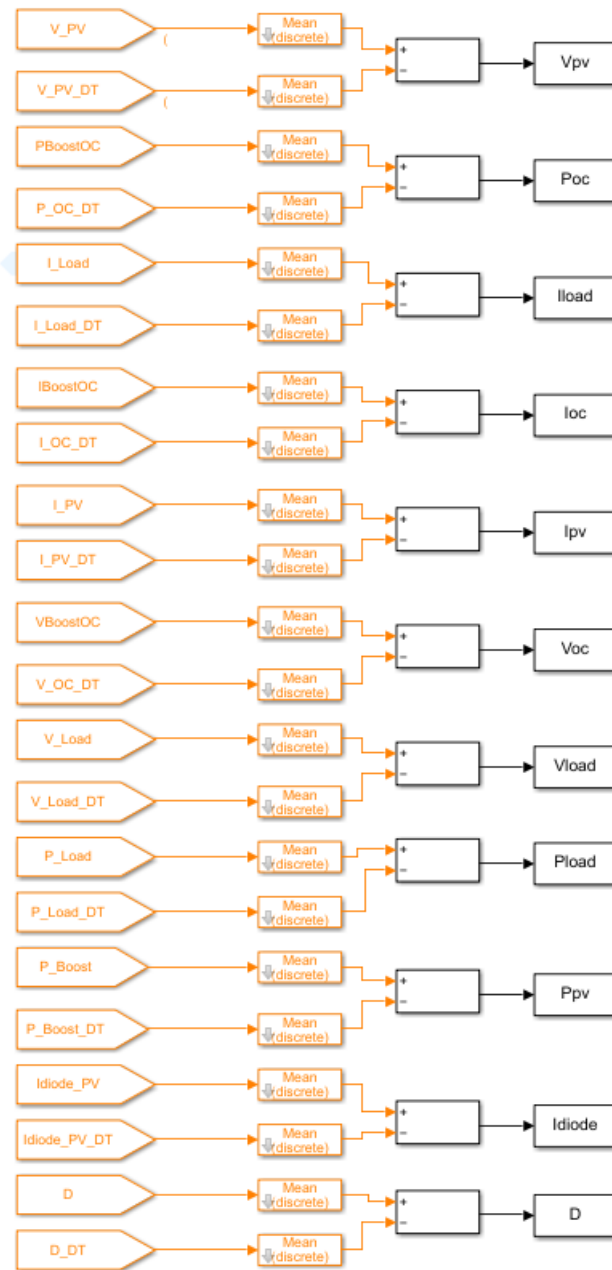


Figure 4.11: Data study for the DT.

change the most.

The built Digital Twin has two functioning modes for fault detection: fixed load and fixed irradiance. In the case of the fixed irradiance, the simulation parameters were kept as in section 4.1, with a temperature of 25°C and an irradiance of $1000 \text{ W}/\text{m}^2$. In the second method, the load was fixed at 20Ω and the same temperature of 25 °C was maintained. In Table 4.13 the simulation parameters are summarized.

Table 4.13: DT simulation parameters.

DT mode	Temperature (°C)	Irradiance (W/m^2)	Load (Ω)
Fixed Load	25	1000, 800, 500, 300	20
Fixed Irradiance	25	1000	20, 30, 40, 50

4.2.1 Cable Fault

As done previously, cable fault diagnosis was performed first. The same method used for the signal-based algorithm was applied for the DT: Different simulations were performed and the changes of all variables were analysed.

Starting with the DT with fixed irradiance, the "transition" periods of all variables when a cable fault occurs are shown in Table 4.14. It is quickly noticed that the difference in the values has a wider range compared to the signal-based algorithm, which translates into a more effective algorithm and, in some cases, a wider gap. The diagnostic variables chosen for this fault were V_{PV} , P_{Load} , V_{Load} , V_{OC} , and I_{Load} .

After the study has been performed for the evolution of each selected diagnostic variable, the obtained conditions can be seen in Table 4.15. The implementation in Simulink is also shown in Figure 4.12, where the algorithm is able to detect the fault running a simulation with $R_{Load} = 20\Omega$.

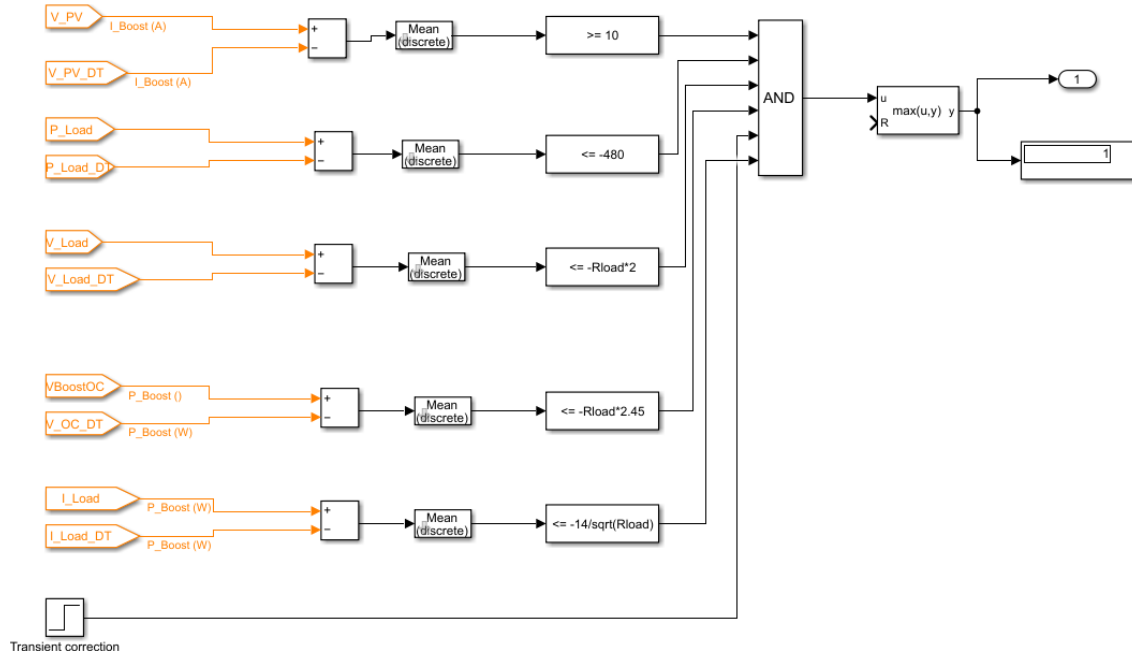


Figure 4.12: Implementation of cable fault algorithm for DT with fixed irradiance.

The same method was used for the fixed load DT. The results obtained after performing the simulations with different irradiances while maintaining the load of 20Ω were as follows in Table 4.16.

Table 4.14: Cable fault simulation results.

Load (Ω)	Transition_D	Transition_ I_{Diode}	Transition_ I_{Load}	Transition_ I_{OC}
20	-0,002979921	9,562588551	-3,531883262	0,008173391
30	-0,003998817	9,524078437	-2,821384708	0,01420033
40	0,080233688	-0,188916342	-2,380835296	0,018924333
50	-0,00303573	9,600152428	-2,072086494	0,021608718

Load (Ω)	Transition_ I_{PV}	Transition_ P_{Load}	Transition_ P_{OC}	Transition_ P_{PV}
20	0,23354604	-503,5433215	-0,098516549	121,767216
30	0,271345248	-500,1944482	-0,151639269	122,2234959
40	-9,610298032	-493,3297033	-0,20200306	-1136,178845
50	0,194993422	-485,0971281	-0,253362017	122,8742978

Load (Ω)	Transition_ V_{Load}	Transition_ V_{OC}	Transition_ V_{PV}
20	-70,63766525	-87,17947994	10,81607982
30	-84,64154124	-101,1157636	10,37715969
40	-95,23341186	-116,3463257	11,44451185
50	-103,6043247	-124,9083759	11,42713633

Table 4.15: Cable fault algorithm in DT with fixed irradiance.

Diagnostic Variable	Load (Ω)	Measured Values	Condition	Condition Values
I_{Load}	20	-3.531883262	$< -13/\sqrt{R_{Load}}$	-2
	30	-2.821384708		-3
	40	-2.380835296		-4
	50	-2.072086494		-5
P_{Load}	20	-503.5433215	< -480	-480
	30	-500.1944482		-480
	40	-493.3297033		-480
	50	-485.0971281		-480
V_{Load}	20	-70.63766525	$< -R_{Load}*2$	-40
	30	-84.64154124		-60
	40	-95.23341186		-80
	50	-103.6043247		-100
V_{OC}	20	-87.17947994	$< -R_{Load}*2.45$	-49
	30	-101.1157636		-73.5
	40	-116.3463257		-98
	50	-124.9083759		-122.5
V_{PV}	20	10.81607982	> 10	10
	30	10.37715969		10
	40	11.44451185		10
	50	11.42713633		10

Table 4.16: Cable fault simulation results with fixed load.

G (W/m^2)	Transition_D	Transition_ I_{Diode}	Transition_ I_{Load}	Transition_ I_{OC}
1000	-0.002979921	9.562588551	-3.531883262	0.008173391
800	0.073274126	0.142551987	-3.12373816	0.004560223
500	0.075683608	0.799640508	-2.03367928	0.002437201
300	0.006400284	1.37579042	-1.220850409	0.001463763

G (W/m^2)	Transition_ I_{PV}	Transition_ P_{Load}	Transition_ P_{OC}	Transition_ P_{PV}
1000	0.23354604	-503.5433215	-0.098516549	121.767216
800	-7.577419272	-394.1354933	-0.079669963	-885.4419416
500	-4.009859296	-167.0980086	-0.033874224	-377.0474486
300	-1.377505066	-60.21870844	-0.012208483	-52.18484715

G (W/m^2)	Transition_ V_{Load}	Transition_ V_{OC}	Transition_ V_{PV}
1000	-70.63766525	-87.17947994	10.81607982
800	-62.47476321	-68.65892621	14.37265123
500	-40.6735856	-43.09778161	34.35579063
300	-24.41700819	-25.8058027	47.8005049

After analysing the evolution of each variable, V_{PV} , P_{Load} , V_{Load} , V_{OC} , and I_{Load} were selected as the variables that evolved most linearly with irradiance and were therefore chosen as diagnostic variables. The summary of all determined conditions for triggering a cable fault warning is shown in Table 4.17. As done with every other fault, a transient correction was maintained for both modes of the DT.

4.2.2 MPPT Fault

The next fault to be investigated was the MPPT fault, since this was the second mode of operation in the MATLAB script. The same simulation study was performed for all variables, as seen in Table 4.18, and for the DT with fixed irradiance the same logic method as in Subsection 4.1.2 was used, meaning that the diagnostic variables were chosen according to the logic that a fault in the MPPT means that current, voltage and power in the load will decrease. In the other mode of operation, the diagnostic variable V_{OC} was added because this fault was triggered when other fault modes were selected in the MATLAB script. Also, a condition stating that the duty cycle returns to its default value of 0.4 was added.

As with the signal-based algorithm, the algorithm has trouble detecting the fault when the load is close to 40Ω because the duty cycle is close to its default value and there is no significant drop in the values measured at the load. However, this is not considered a major setback since the efficiency of the system is maintained and its overall health is not compromised.

Table 4.19 summarizes the determined conditions for this fault for the first mode, with its implementation in Simulink visible in Figure 4.13.

The values of the study done while changing irradiance are also shown in Table 4.20. As mentioned earlier, the diagnostic variables chosen were V_{Load} , I_{Load} , P_{Load} , and V_{OC} .

Table 4.17: Cable fault algorithm for DT with fixed load.

Diagnostic Variable	G (W/m^2)	Measured Values	Condition	Condition Values
V_{PV}	1000	10.81607982	$> 10000/G$	10
	800	14.37265123		12.5
	500	34.35579063		20
	300	47.8005049		33.33333333
P_{Load}	1000	-503.5433215	$< -0.2 * G$	-200
	800	-394.1354933		-160
	500	-167.0980086		-100
	300	-60.21870844		-60
V_{Load}	1000	-70.63766525	$< -G * 0.065$	65
	800	-62.47476321		52
	500	-40.6735856		32.5
	300	-24.41700819		19.5
V_{OC}	1000	-87.17947994	$< -G * 0.075500$	-75
	800	-68.65892621		-60
	500	-43.09778161		-37.5
	300	-25.8058027		-22.5
I_{Load}	1000	-3.531883262	$< -G * 0.003$	-3
	800	-3.12373816		-2.4
	500	-2.03367928		-1.5
	300	-1.220850409		-0.9

Table 4.18: MPPT fault simulation results for DT with fixed irradiance.

Load (W/m^2)	Transition_D	Transition_ I_{Diode}	Transition_ I_{Load}	Transition_ I_{OC}
20	0.112438611	-0.259052975	-0.70950794	-0.011073452
30	0.033189783	-0.278051529	-0.142643594	-0.004779839
40	-0.010984799	0.177247627	-0.009613706	0.001711638
50	-0.044966219	0.821221346	-0.116859118	0.007111442

Load (Ω)	Transition_ I_{PV}	Transition_ P_{Load}	Transition_ P_{OC}	Transition_ P_{PV}
20	0.26226295	-175.6055453	-0.035178554	-198.203248
30	0.278637262	-47.19416708	-0.014166999	-55.63238447
40	-0.17699311	-3.767128919	-0.001532246	-1.938017641
50	-0.819890255	-49.79786169	-0.025111593	-47.45766702

Load (Ω)	Transition_ V_{Load}	Transition_ V_{OC}	Transition_ V_{PV}
20	-14.19015881	-14.10283157	-25.27844291
30	-4.279307812	-4.232447513	-9.643020143
40	-0.384548223	-0.407449615	2.077982583
50	-5.842955901	-5.959700025	5.866068281

Table 4.19: MPPT fault algorithm for DT with fixed irradiance.

Diagnostic Variable	Load (Ω)	Measured Values	Condition	Condition Values
I_{Load}	20	-0.70950794	$< -4/R_{Load}$	-0.2
	30	-0.142643594		-0.133333333
	40	-0.009613706		-0.1
	50	-0.116859118		-0.08
P_{Load}	20	-175.6055453	$< -1500/R_{Load}$	-75
	30	-47.19416708		-50
	40	-3.767128919		-37.5
	50	-49.79786169		-30
V_{Load}	20	-14.19015881	$< -120/R_{Load}$	-6
	30	-4.279307812		-4
	40	-0.384548223		-3
	50	-5.842955901		-2.4

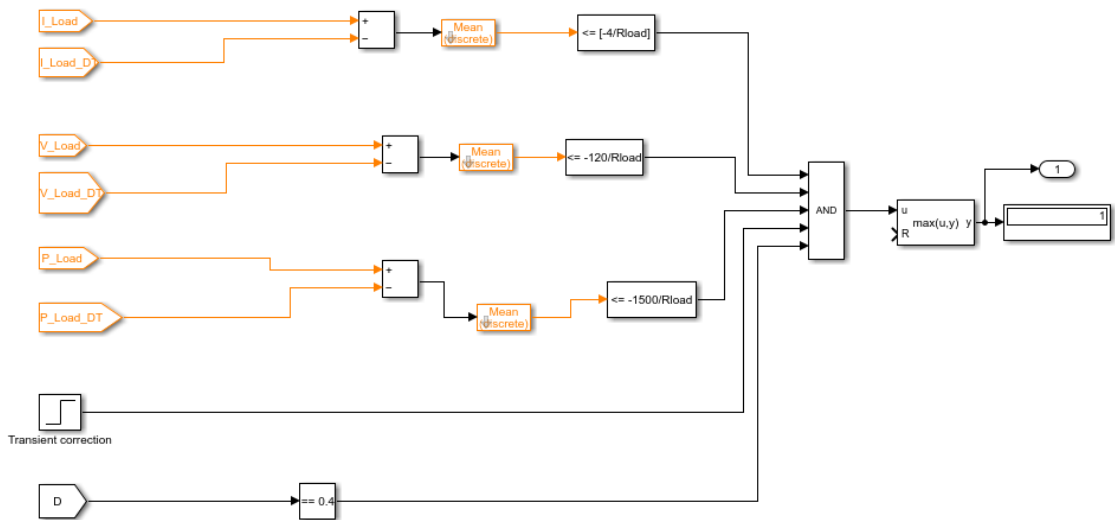


Figure 4.13: Implementation of MPPT fault algorithm for DT with fixed irradiance

Table 4.20: MPPT fault simulation results for DT with fixed load.

Irradiance(W/m^2)	Transition_D	Transition_I_{Diode}	Transition_I_{Load}	Transition_I_{OC}
1000	0.112439	-0.25905	-0.70951	-0.01107
800	0.151401	-0.0759	-0.84925	-0.01091
500	0.161993	-7.7E-05	-0.60756	-0.00725
300	0.162035	-3.2E-07	-0.36495	-0.00435

Irradiance (W/m^2)	Transition_I_{PV}	Transition_P_{Load}	Transition_P_{OC}	Transition_P_{PV}
1000	0.262263	-175.606	-0.03518	-198.203
800	0.079228	-178.056	-0.03564	-202.068
500	0.001595	-81.5614	-0.01632	-92.667
300	0.000547	-29.4077	-0.00589	-33.4104

Irradiance (W/m^2)	Transition_V_{Load}	Transition_V_{OC}	Transition_V_{PV}
1000	-14.1902	-14.1028	-25.2784
800	-16.9849	-16.8897	-29.3007
500	-12.1512	-12.0857	-20.6727
300	-7.29905	-7.25979	-12.4129

Table 4.21 shows the conditions studied to trigger this fault warning.

4.2.3 SC Fault

In this subsection, the algorithm for diagnosing a short-circuit fault in the transistor is presented. As before, simulations were performed with different loads with an irradiance of $1000W/m^2$ and different irradiances with a load of 20Ω . First, the method for fixed irradiances is explained. The simulation study performed is shown in Table 4.22.

Again, the diagnostic variables that evolve most linearly as a function of the evolution of the selected load were chosen. Thus, P_{PV} , V_{PV} , V_{Load} , V_{OC} were chosen for the reasons mentioned above.

The same procedure was followed, in which case a fixed load was maintained while the irradiance changed. The results obtained in the simulations are shown in Table 4.24.

After analysing the results, the variables that showed a reasonably linear trend and were therefore selected as diagnostic variables were as shown in Table 4.25. This was the algorithm obtained for the DT with fixed load.

In image 4.14 it is shown the implementation of the algorithm for the DT with fixed load in Simulink.

4.2.4 OC Fault

Following the same procedures as before, the data were analysed for an OC fault after simulations were performed for a fixed irradiance. A summary of all variables during the transition period is shown in Table 4.26.

Table 4.21: MPPT fault algorithm in DT with fixed load.

Diagnostic Variable	G (W/m^2)	Measured Values	Condition	Condition Values
V_{PV}	1000	-25.27844291	$< -0.014 * G$	-25
	800	-29.30070869		-20
	500	-20.67267349		-12.5
	300	-12.41293458		-7.5
P_{Load}	1000	-175.6055453	$< -0.09 * G$	-90
	800	-178.0557239		-72
	500	-81.56137081		-45
	300	-29.40773766		-27
V_{Load}	1000	-14.19015881	$< -G * 0.014$	-14
	800	-16.98492283		-11.2
	500	-12.15117165		-7
	300	-7.299051281		-4.2
V_{OC}	1000	-14.10283157	$< -G * 0.014$	-14
	800	-16.88969021		-11.2
	500	-12.08573634		-7
	300	-7.259789422		-4.2

Table 4.22: SC fault simulation results for DT with fixed irradiance.

Load (Ω)	Transition_D	Transition_ I_{Diode}	Transition_ I_{Load}	Transition_ I_{OC}
20	-0.05015	-0.25313	-3.66866	0.0064128
30	-0.12107	-0.28974	-2.93	0.0124028
40	-0.16034	-0.20946	-2.47259	0.0171349
50	-0.19077	-0.23162	-2.14776	0.0197807
Load (Ω)	Transition_ I_{PV}	Transition_ P_{Load}	Transition_ P_{OC}	Transition_ P_{PV}
20	0.261474	-521.098	-0.10591	-5.13E+02
30	0.297746	-517.805	-0.15992	-5.12E+02
40	0.21739	-510.823	-0.2131	-5.12E+02
50	0.239423	-501.212	-0.265	-5.11E+02
Load (Ω)	Transition_ V_{Load}	Transition_ V_{OC}	Transition_ V_{PV}	
20	-73.3731	-76.4125	-60.2651	
30	-87.8999	-93.9625	-60.6374	
40	-98.9034	-108.523	-59.5671	
50	-107.388	-121.049	-59.7398	

Table 4.23: SC fault algorithm for DT with fixed irradiance.

Diagnostic Variable	Load (Ω)	Measured Values	Condition	Condition Values
I_{PV}	20	0.261474193	> 0.2	0.2
	30	0.297745543		0.2
	40	0.217389729		0.2
	50	0.239422597		0.2
P_{Load}	20	-521.09792	< -500	-500
	30	-517.8049453		-500
	40	-510.8232093		-500
	50	-501.2119222		-500
P_{OC}	20	-0.105913495	$< -R_{Load} * 0.004$	0.08
	30	-0.159916712		-0.12
	40	-0.213100393		-0.16
	50	-0.26500218		-0.2
P_{PV}	20	-87.17947994	< -500	-500
	30	-101.1157636		-500
	40	-116.3463257		-500
	50	-124.9083759		-500
V_{Load}	20	-73.37314289	$< -R_{Load} * 2$	-40
	30	-87.89992376		-60
	40	-98.90344166		-80
	50	-107.3881052		-100
V_{OC}	20	-76.41250723	$< -R_{Load} * 2.3$	-46
	30	-93.96253178		-69
	40	-108.5226763		-92
	50	-121.0492349		-115
V_{PV}	20	-60.26506376	< -55	-55
	30	-60.63744279		-55
	40	-59.56713856		-55
	50	-59.73982522		-55

Table 4.24: SC fault simulation results for DT with fixed load.

Irradiance (W/m^2)	Transition_D	Transition_I_{Diode}	Transition_I_{Load}	Transition_I_{OC}
1000	-0.05015	-0.25313	-3.66866	0.006413
800	-0.01526	-0.07265	-3.24668	0.003014
500	-0.00571	-7.1E-05	-2.11419	0.00143
300	-0.00568	-2.9E-07	-1.26918	0.000858

Irradiance (W/m^2)	Transition_I_{PV}	Transition_P_{Load}	Transition_P_{OC}	Transition_P_{PV}
1000	0.261474	-521.098	-0.10591	-513.051
800	0.079331	-408.113	-0.08293	-407.296
500	0.002907	-173.057	-0.03516	-173.331
300	0.001022	-62.3663	-0.01267	-62.4523

Irradiance (W/m^2)	Transition_V_{Load}	Transition_V_{OC}	Transition_V_{PV}
1000	-73.3731	-76.4125	-60.2651
800	-64.9336	-67.5855	-57.8032
500	-42.2839	-44.0024	-38.626
300	-25.3837	-26.4153	-23.1882

Table 4.25: SC fault algorithm in DT with fixed load.

Diagnostic Variable	G (W/m^2)	Measured Values	Condition	Condition Values
V_{PV}	1000	-60.26506376	$< -G * 0.059$	-59
	800	-57.80315141		-47.2
	500	-38.62601316		-29.5
	300	-23.18822154		-17.7
P_{Load}	1000	-521.09792	$< -0.2 * G$	-200
	800	-408.1132778		-160
	500	-173.057101		-100
	300	-62.36626669		-60
V_{Load}	1000	-73.37314289	$< -G * 0.07$	-70
	800	-64.93357461		-56
	500	-42.28386646		-35
	300	-25.38369229		-21
V_{OC}	1000	-76.41250723	$< -G * 0.07$	-70
	800	-67.58545117		-56
	500	-44.00236401		-35
	300	-26.41534001		-21
P_{PV}	1000	-513.0514214	$< -G * 0.2$	-200
	800	-407.2959518		-160
	500	-173.3311512		-100
	300	-62.45227433		-60

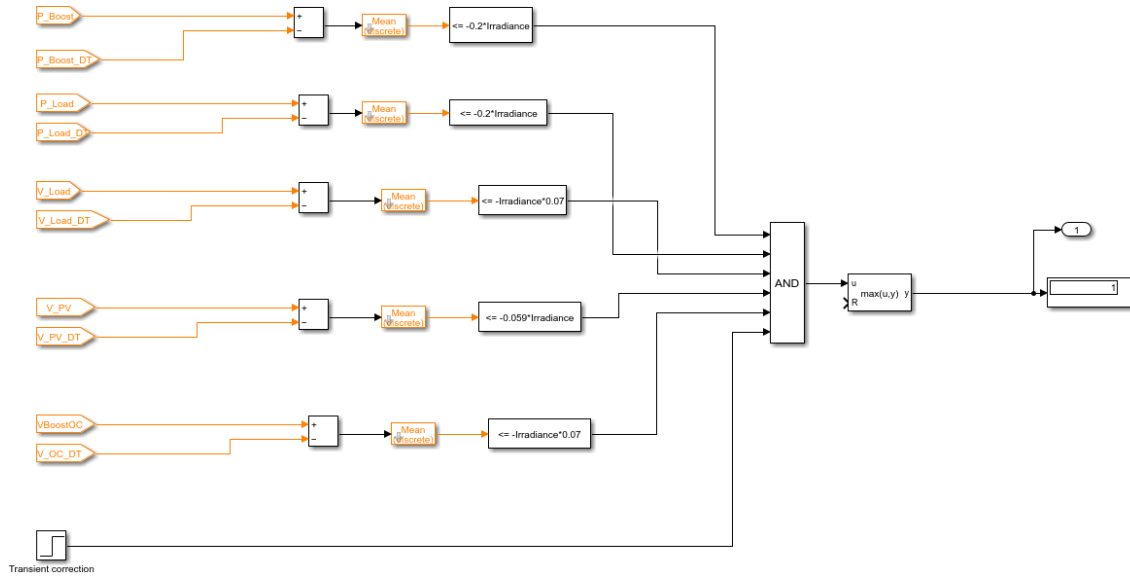


Figure 4.14: Implementation of SC algorithm for DT with fixed load.

Table 4.26: OC fault simulation results for DT with fixed irradiance.

Load (Ω)	Transition_D	Transition_ I_{Diode}	Transition_ I_{Load}	Transition_ I_{OC}
20	0.004464	1.278581	-0.43388	0.008618
30	0.076043	0.370585	-0.79307	0.014619
40	-0.01162	5.79418	-0.93649	0.019353
50	-0.00758	6.565504	-0.97236	0.021998

Load (Ω)	Transition_ I_{PV}	Transition_ P_{Load}	Transition_ P_{OC}	Transition_ P_{PV}
20	-1.2795	-113.031	-0.08507	-94.3119
30	-4.25763	-233.456	-0.13741	-461.586
40	-0.18791	-299.845	-0.19009	64.95007
50	-0.07926	-334.979	-0.24192	78.82868

Load (Ω)	Transition_ V_{Load}	Transition_ V_{OC}	Transition_ V_{PV}
20	-8.67765	-42.5468	7.340569
30	-23.7921	-58.8305	8.883311
40	-37.4595	-73.2262	10.35778
50	-48.6178	-85.6822	10.44287

Table 4.27: OC fault algorithm for DT with fixed irradiance

Diagnostic Variable	Load (Ω)	Measured Values	Condition	Condition Values
I_{Load}	20	-0.433882462	$MAX(I_{Load}) < 1$	1
	30	-0.793069938		1
	40	-0.936487196		1
	50	-0.972356712		1
P_{Load}	20	-113.0310796	$< -R_{Load} * 5$	-100
	30	-233.4563107		-150
	40	-299.8454938		-200
	50	-334.9785769		-250
V_{Load}	20	-8.677649249	$< -R_{Load} * 0.4$	-8
	30	-23.79209814		-12
	40	-37.45948783		-16
	50	-48.6178356		-20
V_{OC}	20	-42.54683736	$< -R_{Load} * 1.5$	-30
	30	-58.83045841		-45
	40	-73.226203		-60
	50	-85.68218507		-75
V_{PV}	20	10.81607982	> 7	7
	30	10.37715969		7
	40	11.44451185		7
	50	11.42713633		7

The diagnostic variables chosen for this fault were P_{Load} , V_{Load} , V_{OC} , and V_{PV} . As can be seen from the results, the first three decrease the most, with the difference increasing at higher load, while V_{PV} is the only one that increases at any load, having a higher difference at the highest load. In addition, only in the cable fault V_{PV} shows an increase, so this variable was more important in distinguishing between faults.

After analysing the evolution of the selected diagnostic variables with the increase of the load, the conditions presented in Table 4.27 result as parameters for an OC fault warning.

Subsequently, the same procedure was made with respect to the other mode of operation of the DT: fixed load and variable irradiance. Table 4.28 shows the data study performed for this fault.

As the analysis of the data results shows, there are not many parameters that evolve linearly and in a higher order of magnitude relative to other variables. Nevertheless, it was still possible to create an algorithm that identifies this type of fault, although some of the most undesirable variables were selected as diagnostic variables. As mentioned before, the "OC" and "SC" measurements are not always easy to measure in practise, since these terminals are not always available. Still, the chosen diagnostic variables were I_{OC} , P_{OC} , V_{OC} , V_{Load} and V_{PV} .

Table 4.29 lists the conditions that were identified as parameters for diagnosing this type of fault. Naturally, the magnitude of these functions is also much smaller than the previous algorithms, since these diagnostic variables change much less rapidly compared to the other faults.

An example of the OC algorithm for the DT with fixed irradiance is shown in Figure 4.15

Table 4.28: OC fault simulation results for DT with fixed load.

Irradiance (W/m^2)	Transition_D	Transition_ I_{Diode}	Transition_ I_{Load}	Transition_ I_{OC}
1000	0.004464	1.278581	-0.43388	0.008618
800	0.002706	0.594702	-0.13031	0.004895
500	0.000891	0.002185	0.203369	0.002668
300	0.000869	2.13E-06	0.123336	0.001602

Irradiance (W/m^2)	Transition_ I_{PV}	Transition_ P_{Load}	Transition_ P_{OC}	Transition_ P_{PV}
1000	-1.2795	-113.031	-0.08507	-94.3119
800	-0.59543	-31.2845	-0.06375	-17.7315
500	-0.00291	34.4394	-0.02464	44.10154
300	-0.00026	12.54504	-0.00887	16.04204

Irradiance (W/m^2)	Transition_ V_{Load}	Transition_ V_{OC}	Transition_ V_{PV}
1000	-8.67765	-42.5468	7.340569
800	-2.60616	-35.097	7.477316
500	4.067385	-19.9655	9.890936
300	2.466718	-11.9731	5.963564

Table 4.29: OC fault algorithm for DT with fixed load.

Diagnostic Variable	G (W/m^2)	Measured Values	Condition	Condition Values
I_{OC}	1000	0.008618251	$< -G * 4E-7$	0.004
	800	0.004894922		0.0032
	500	0.002667953		0.002
	300	0.001601747		0.0012
P_{OC}	1000	-0.085065397	$< -G * 75E-8$	-0.0075
	800	-0.063745432		-0.006
	500	-0.024640487		-0.00375
	300	-0.008873233		-0.00225
V_{Load}	1000	-8.677649249	$MAX(V_{Load}) < 10$	10
	800	-2.606163562		10
	500	4.067385332		10
	300	2.46671765		10
V_{OC}	1000	-42.54683736	$< -G * 0.035$	-35
	800	-35.09699016		-28
	500	-19.96546498		-17.5
	300	-11.97307619		-10.5
V_{PV}	1000	7.34056934	> 5	5
	800	7.477315997		5
	500	9.890936075		5
	300	5.963564494		5

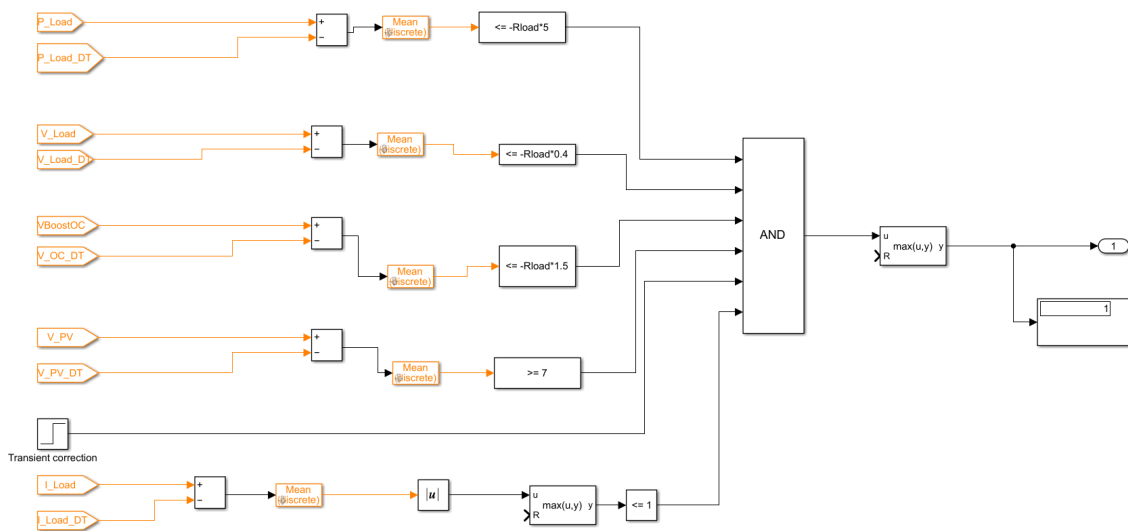


Figure 4.15: Implementation of OC algorithm for DT with fixed irradiance in Simulink.

4.2.5 Intermittence fault

As before, the intermittence fault was the last to be studied. The data study for the digital twin with fixed irradiance is shown in Table 4.30.

In this case, I_{OC} is one of the variables that would be chosen in any case if it were not for the premise that it should be avoided. In contrast to the case in section 4.1.5, there are many other variables that meet the requirements to be selected as diagnostic variables. With this in mind, the diagnostic variables P_{PV} , V_{PV} , P_{Load} , V_{Load} , and V_{OC} were selected. A threshold of maximum difference of 27 with respect to V_{Load} was set to distinguish intermittence and SC faults.

Table 4.31 shows the calculated functions of the evolution of the selected diagnostic variables in order to identify this fault.

With respect to the DT with fixed load, the same procedure was followed. Table 4.32 shows the results of the data study performed. As in the fixed irradiance case, I_{OC} was avoided and a threshold of 27 was applied to the difference of V_{Load} .

The final algorithm corresponds to the Table 4.33, and its implementation in Simulink is shown in Figure 4.16.

Table 4.30: Intermittence fault simulation results for DT with fixed irradiance.

Load (Ω)	Transition_D	Transition_ I_{Diode}	Transition_ I_{Load}	Transition_ I_{OC}
20	-0.00387	-0.2597	-1.19491	2.556457
30	-0.00333	-0.28549	-0.55633	2.609307
40	-6.91E-04	-0.17257	-0.20822	2.62186
50	2.33E-06	0.010084	-0.05838	2.532704

Load (Ω)	Transition_ I_{PV}	Transition_ P_{Load}	Transition_ P_{OC}	Transition_ P_{PV}
20	0.264032	-269.516	-0.05266	-267.036
30	0.287713	-168.697	-0.07683	-158.418
40	0.173097	-77.5445	-0.0935	-59.7847
50	-0.01086	-24.8709	-0.11251	-2.56006

Load (Ω)	Transition_ V_{Load}	Transition_ V_{OC}	Transition_ V_{PV}
20	-23.8983	-48.6558	-32.9646
30	-16.69	-54.2373	-21.1854
40	-8.32863	-57.7005	-8.74879
50	-2.91881	-61.6503	-0.12803

Table 4.31: Intermittence fault algorithm for DT with fixed irradiance.

Diagnostic Variable	Load (Ω)	Measured Values	Condition	Condition Values
P_{PV}	20	-267.0358309	$< -2250/R_{Load}$	-112.5
	30	-158.4180823		-75
	40	-59.78474225		-56.25
	50	-2.560055555		-45
P_{Load}	20	-269.5160407	$< -3000/R_{Load}$	-150
	30	-168.6972446		-100
	40	-77.54446035		-75
	50	-24.87087725		-60
V_{Load}	20	-23.89826576	$< -300/R_{Load}$	-15
	30	-16.68997288		-10
	40	-8.328631798		-7.5
	50	-2.918810863		-6
V_{OC}	20	-48.65577274	$< -R_{Load}*1.4$	-28
	30	-54.23730445		-42
	40	-57.70049921		-56
	50	-61.6503462		-70
V_{PV}	20	-32.96457405	$< 325/R_{Load}$	-16.25
	30	-21.18544365		-10.83333333
	40	-8.748789733		-8.125
	50	-0.128033194		-6.5
I_{OC}	20	2.556456798	> 2	2
	30	2.609306924		2
	40	2.621860049		2
	50	2.532704215		2

Table 4.32: Intermittence fault simulation results for DT with fixed load.

Irradiance (W/m^2)	Transition_D	Transition_I_{Diode}	Transition_I_{Load}	Transition_I_{OC}
1000	-0.00387	-0.2597	-1.19491	2.556457
800	-0.00348	-0.07618	-1.23805	2.037075
500	-0.0028	-7.7E-05	-0.85056	1.272827
300	-0.0028	-3.2E-07	-0.51072	0.763858

Irradiance (W/m^2)	Transition_I_{PV}	Transition_P_{Load}	Transition_P_{OC}	Transition_P_{PV}
1000	0.264032	-269.516	-0.05266	-267.036
800	0.080211	-238.242	-0.04744	-245.199
500	0.001869	-105.138	-0.02104	-109.434
300	0.000646	-37.8963	-0.00758	-39.444

Irradiance (W/m^2)	Transition_V_{Load}	Transition_V_{OC}	Transition_V_{PV}
1000	-23.8983	-48.6558	-32.9646
800	-24.7611	-44.8589	-35.3166
500	-17.0111	-29.6614	-24.4098
300	-10.2144	-17.8082	-14.6535

Table 4.33: Intermittence fault algorithm for DT with fixed load.

Diagnostic Variable	G (W/m^2)	Measured Values	Condition	Condition Values
P_{Load}	1000	-269.5160407	< -0.12*G	-120
	800	-238.2424593		-96
	500	-105.1383147		-60
	300	-37.89633444		-36
P_{PV}	1000	-267.0358309	< -G*0.12	-120
	800	-245.1992666		-96
	500	-109.433513		-60
	300	-39.44401819		-36
V_{Load}	1000	-23.89826576	< -G*0.02	-20
	800	-24.76108144		-16
	500	-17.01111465	AND	-10
	300	-10.2143921	Max($ V_{Load} $) < 27	-6
V_{OC}	1000	-48.65577274	< -G*0.04	-40
	800	-44.85887918		-32
	500	-29.66137589		-20
	300	-17.80822572		-12
V_{PV}	1000	-32.96457405	< -G*0.03	-30
	800	-35.31655084		-24
	500	-24.40981264		-15
	300	-14.65352641		-9

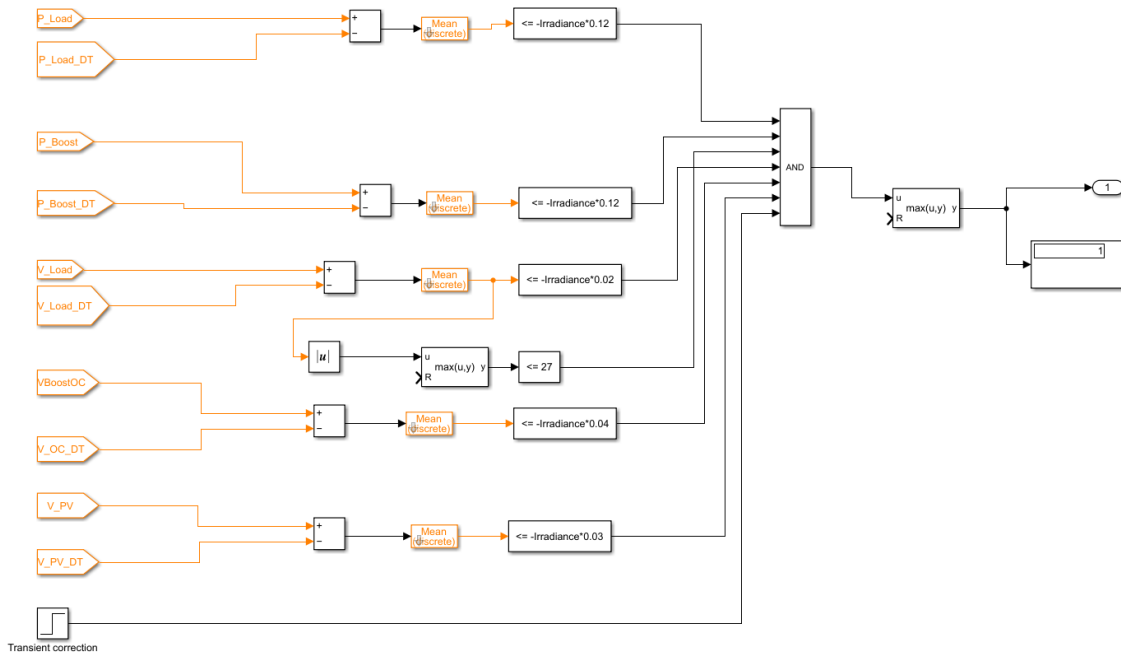


Figure 4.16: Implementation of Intermittence fault algorithm in DT with fixed load.

Chapter 5

Algorithm Evaluation

In this chapter, the strength of the algorithms is evaluated by two different methods. First, the unwanted variables will be removed from the signal-based algorithm explained in Section 4.1. Then, a noise evaluation procedure is performed to determine how much noise power can be added without affecting the algorithms.

5.1 Variable Analysis

Some of the diagnostic variables chosen in this project are not ideal, but were necessary to be able to distinguish between faults and not receive false warnings when a different type of fault is introduced into the system. Although both "SC" and "OC" measurements were avoided, they were still necessary for this project. Therefore, a study was conducted to evaluate exactly how relevant each variable was to the design of this project.

This was done for the three different methods used in this dissertation. Table 5.1 lists the most used variables for the signal-based algorithm, the DT with fixed irradiance and the DT with fixed load.

The analysis of the obtained results shows that V_{Load} is the most important diagnostic variable that appears in literally every single fault algorithm. As for the problematic variables, V_{OC} appears very frequently compared to the other variables (12 times). On average, all used variables appear 7.89 times in all algorithms, so V_{OC} has an above average usage rate and ranks tied for third place. I_{OC} , V_{SC} and P_{OC} appear a total of 6 times in all algorithms, which is not a particularly high frequency, but is still important. Between OC /SC voltage and current, the more problematic to measure is usually current, and only in one instance it is used.

I_{Diode} , Duty Cycle, I_{SC} , P_{SC} , and I_{PV} were not used as diagnostic variables in any of the algorithms for the selected faults.

Figure 5.1 shows a bar graph of the use of each variable for all algorithms.

Table 5.1: Variable usage between all algorithms

	Diagnostic variable	Algorithm appearances	Total
Signal-Based	V_{Load}	Cable, MPPT, SC, OC, Intermittence	5
	P_{Load}	Cable, MPPT, SC, OC, Intermittence	5
	V_{PV}	Cable, OC, Intermittence	3
	V_{OC}	SC, OC, Intermittence	3
	V_{SC}	SC, OC, Intermittence	3
	I_{Load}	Cable, MPPT	2
	P_{PV}	SC, Intermittence	2
	I_{OC}	OC	1
DT fixed irradiance	V_{Load}	Cable, MPPT, SC, OC, Intermittence	5
	P_{Load}	Cable, MPPT, SC, OC, Intermittence	5
	V_{PV}	Cable, SC, OC, Intermittence	4
	V_{OC}	Cable, SC, OC, Intermittence	4
	I_{Load}	Cable, MPPT, OC	3
	P_{PV}	SC, Intermittence	2
	DT fixed load	V_{Load}	Cable, MPPT, SC, OC, Intermittence
V_{PV}		Cable, MPPT, SC, OC, Intermittence	5
V_{OC}		Cable, MPPT, SC, OC, Intermittence	5
P_{Load}		Cable, MPPT, SC, Intermittence	4
P_{PV}		SC, Intermittence	2
I_{OC}		OC	1
I_{Load}		Cable	1
P_{OC}		OC	1

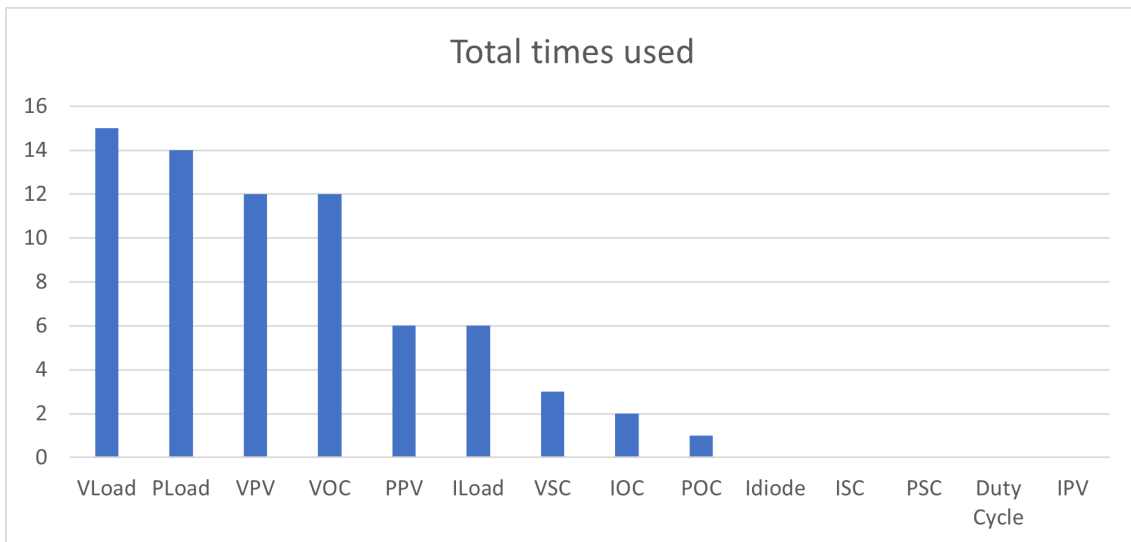


Figure 5.1: Variable usage in all algorithms

5.2 Testing of algorithms without undesirable diagnostic variables

In order to test the need of the "OC" and "SC" variables, they were removed from the algorithms to determine if they still work as they should. Starting with the Signal-Based algorithm, looking at Table 5.1 this algorithm uses V_{OC} , V_{SC} and I_{OC} . Since these values are not always easy to measure, these were simply deleted from the algorithm to simulate the inability to access them.

To test the viability of the algorithm, every fault was introduced in the system with a load of 30Ω . Irradiance and temperature were maintained at $1000W/m^2$ and $25^\circ C$, respectively.

As an example of the implementation of the OC algorithm in Simulink is shown in Figure 5.2. As mentioned earlier, the only difference from the previous version is that the unwanted diagnostic variables V_{SC} , V_{OC} , and I_{OC} have been removed.

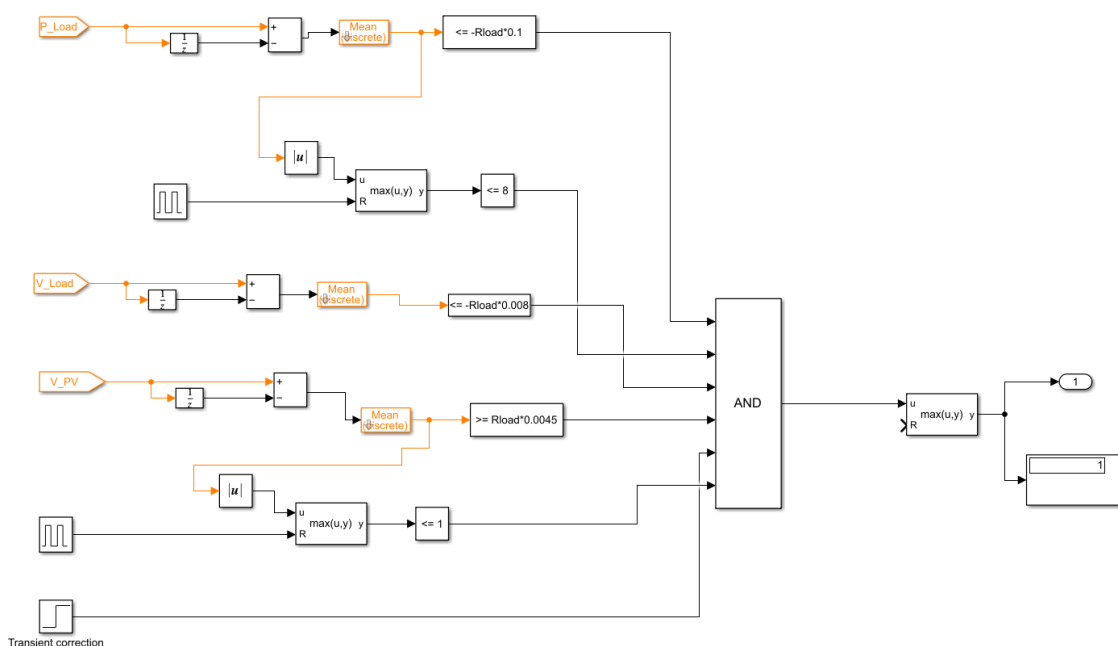


Figure 5.2: Implementation of OC algorithm with less variables in Simulink

Since the undesirable variables were selected as diagnostic variables for the algorithms only for the OC, SC, and intermittence faults, it is expected that both cable and MPPT algorithms will work as usual.

After running simulations for every mode, only two of them were problematic. When a cable fault was introduced, a OC warning was also triggered, resulting in a false positive on the first simulation attempt, as shown in Figure 5.3.

When analysing both algorithms, this behaviour is easily justified. When the unwanted diagnostic variables are removed, the OC algorithm is controlled with only V_{Load} , V_{PV} , and P_{Load} . All of these variables are used in the cable algorithm, and their behaviour is similar: P_{Load} and V_{Load} decrease, while V_{PV} increases by similar amounts.

Modes 2, 3, and 4 were still functional and did not exhibit false positives/negatives. However, when an intermittence fault was introduced into the system, a false positive warning of a OC

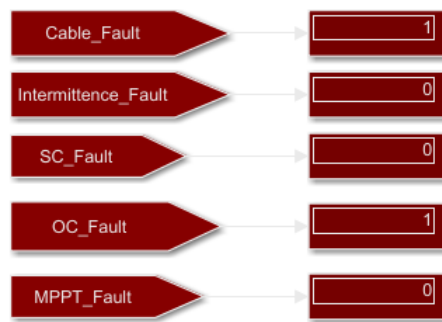


Figure 5.3: Fault warnings when a Cable fault was introduced without the undesirable diagnostic variables for the Signal-Based algorithm.

fault was again triggered as seen in Figure 5.4. Comparing their diagnostic variables without the unwanted ones, both have V_{Load} , P_{Load} , and V_{PV} , with the intermittence algorithm having an additional variable in P_{PV} .

Comparing the behaviour of the diagnostic variables that these algorithms have in common, both P_{Load} and V_{Load} have similar conditions that decrease in the same order of magnitude as each fault occurs. However, in a simple analysis of the Tables 4.10 and 4.12, no false positive OC warning is expected, since in one case V_{PV} increases (OC) and in the other case it decreases (intermittence).

A closer look at the graph of the V_{PV} difference (Figure 5.5) when there is an intermittence fault in the system shows that the difference has a positive spike around 0.52 seconds into the simulation and higher than the condition set for the OC algorithm. This triggers the warning, since every other diagnostic variable behaves as if there is such a fault in the system. This behaviour is easily explained as an intermittence fault is due to a bad connection and is expected to be irregular and inconstant, changing from a "good" to a "bad" connection in a few microseconds, as modelled in this system.

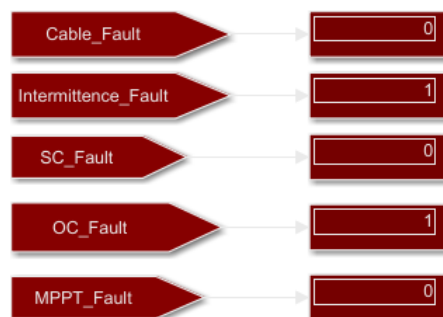


Figure 5.4: Fault warnings when an Intermittence fault was introduced without the undesirable diagnostic variables for the Signal-Based algorithm.

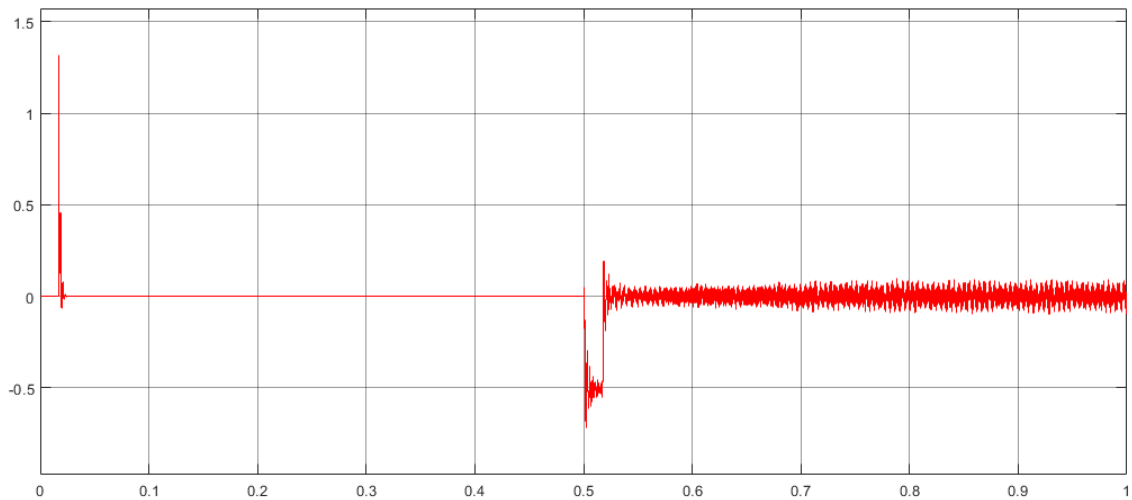


Figure 5.5: Difference in diagnostic variable V_{PV} with an Intermittence fault in the system.

The same procedure was performed for the digital twin with fixed irradiance. The simulation parameters were kept, with a constant irradiance of $1000W/m^2$ and a temperature of $25^{\circ}C$.

In the algorithms for DT, only the MPPT does not have any of the undesirable diagnostic variables, as the rest of them all include V_{OC} .

Simulations were performed for all faults with a load of 30Ω . No problems were encountered with the first mode of simulation. When an MPPT fault was introduced into the system, as shown in Figure 5.6, a false positive was triggered by the algorithm, being in this case an intermittence fault warning. These algorithms share P_{Load} and V_{Load} as diagnostic variables and show the same behaviour for both faults. P_{PV} and V_{PV} are the remaining diagnostic variables for an intermittence fault and both decrease when both faults occur. These were not chosen as diagnostic variables because their evolution is not linear with the load for the MPPT fault, but for this load the difference in value was sufficient for a warning of an intermittence fault.

When a SC fault was introduced into the system, the algorithm was also unable to correctly identify the faults. While the correct fault was identified, an intermittence fault warning was

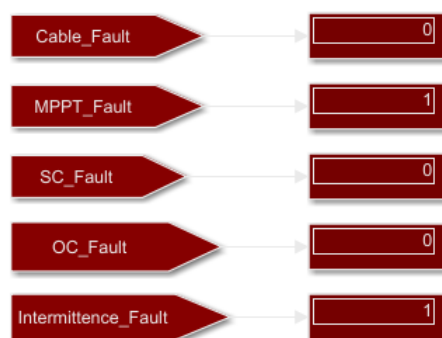


Figure 5.6: Fault warnings when an MPPT fault was introduced without the undesirable diagnostic variables for DT with fixed irradiance.

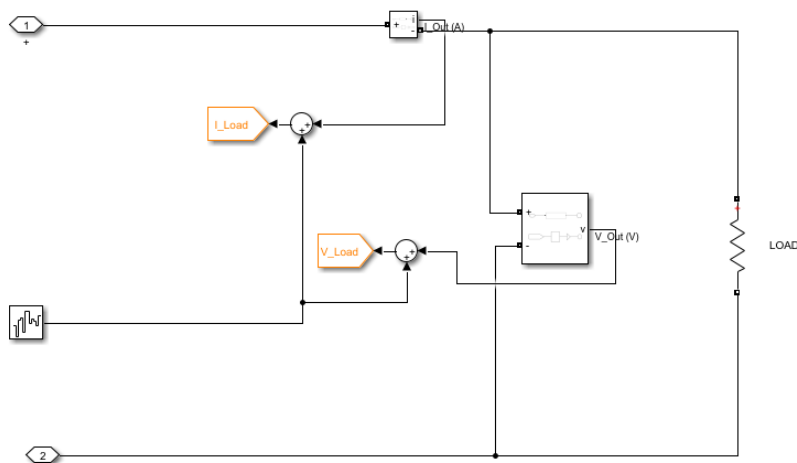


Figure 5.7: Illustration of the addition of white noise in Simulink.

also triggered. Looking at the diagnostic variables of the two algorithms, they share P_{PV} , V_{Load} , V_{PV} and P_{Load} , with the SC algorithm also having I_{PV} . All the shared variables show the same behaviour, since they decrease when both faults occur. This common behaviour justifies the fact that a false positive warning is triggered without the undesirable diagnostic variables responsible for distinguishing between the faults.

From this analysis, it can be concluded that although the measurements may be difficult, they are necessary for this digital twin and signal-based algorithm approach, at least when they are intended to detect multiple faults.

5.3 Noise Evaluation

As another method of evaluating the strength of the algorithms, noise was added to the measurements of all variables in the system. This was done using the Band Limited White Noise block in Simulink, as shown in the example in Figure 5.7. This study is about seeing how strong the algorithms are and how much interference they can withstand while still being able to correctly identify the faults. Although real measurements are not subject to white noise, this is a good theoretical approximation to real noise interference, which has a correlation time that is very small relative to the natural bandwidth of the system. [24] This test was performed only for DT with fixed irradiance and with the signal-based algorithm, since the same conditions of irradiance and temperature apply to both.

The procedure of this study began with adding a small amount of noise to each measurement, analysing the true and false positive/negative warnings, and then increasing the noise power when the algorithms were still able to function properly until they no longer did.

In order to have a reliable method of comparison, the same procedure was used for both algorithms. Simulations were performed for loads of 20, 30, 40, and 50 Ω while increasing noise power at the same rate, analysing the number of true and false positives/negatives results after

Table 5.2: Noise study example.

Noise power ($\text{mag}^2/(\text{rad}/\text{sec})$)		Introduced Fault	TP	TN	FP	FN
Load = 20 Ω	50	No fault	0	5	0	0
		Cable Fault	0	3	1	1
		MPPT	1	4	0	0
		SC Gate	1	4	0	0
		OC Gate	0	4	0	1
		Intermittence	0	3	1	1
Load = 30 Ω	50	No fault	0	5	0	0
		Cable Fault	0	3	1	1
		MPPT	1	4	0	0
		SC Gate	1	4	0	0
		OC Gate	0	4	0	1
		Intermittence	0	4	0	1
Load = 40 Ω	50	No fault	0	5	0	0
		Cable Fault	0	3	1	1
		MPPT	1	4	0	0
		SC Gate	1	4	0	0
		OC Gate	0	4	0	1
		Intermittence	0	4	0	1
Load = 50 Ω	50	No fault	0	5	0	0
		Cable Fault	0	3	1	1
		MPPT	1	4	0	0
		SC Gate	1	4	0	0
		OC Gate	0	4	0	1
		Intermittence	0	4	0	1

each simulation. In Simulink, the noise power parameter corresponds to the height of the power spectral density generated by the function block.

As an example, an excerpt from the study for the signal-based algorithm is shown in Table 5.2. For both algorithms, the noise power began at 0.1, increasing to 1, 10, 20, and ended at 50. This was chosen as the final measure of noise power because, as can be seen in the table, many of the algorithms began to fail. In this excerpt, the algorithms for cable, OC, and intermittence failed at every load examined. In some cases, incorrect fault warnings were issued, and in other cases the algorithm simply failed to detect the fault implemented into the system. A summary of the noise study performed is shown in Tables 5.3 and 5.4. For each level of noise power, 4 different loads were simulated, each with 6 different simulation modes (one for each fault and one without fault). The perfect value for the number of true positives would be 20 and the number of true negatives would be 25. Comparing the values obtained in the two tables, it can be seen that the DT had a better performance than the signal-based algorithm.

As another method of analysis, a Confusion Matrix was created using the results obtained. A confusion matrix is a performance measurement tool for a problem whose results can be divided into two or more different classes [25]. This allows the algorithm to be evaluated by many different instruments such as precision, accuracy, and F-measure, all of which are used in this chapter. The

Table 5.3: Noise study summary for DT with fixed irradiance.

Noise power ($\text{mag}^2/(\text{rad}/\text{sec})$)	TP	TN	FP	FN
0.1	14	100	0	6
1	15	100	0	5
10	13	100	2	5
20	12	100	1	7
50	12	97	3	8

confusion matrix shows the values of true and false negatives/positives, as illustrated by Figure 5.8.

The comparison of the two confusion matrices shows that the use of a digital twin is a more effective method for fault diagnosis. With this method, there are fewer False Positives, fewer False Negatives, and more True Positives and Negatives, with better overall results in all categories.

Several other comparison metrics were calculated to provide deeper insight into how the methods compare. Starting with Precision, which is a measure of how many of the positive predictions are actually positive. It is calculated according to the formula in Equation 5.1, and if the number of False Positives is low, the Precision is high.

$$P = \frac{TP}{TP + FP} = \frac{\text{Number of Correctly Predicted Positive Instances}}{\text{Number of Positive Predictions}} \quad (5.1)$$

Recall, as seen in equation 5.2, is the percentage of True Positives in agreement with all labeled data. If the number of False Negatives is high, the Recall is low.

$$R = \frac{TP}{TP + FN} = \frac{\text{Number of Correctly Predicted Positive Instances}}{\text{Number of Total Positive Instances in the Dataset}} \quad (5.2)$$

The F1-Score, as seen in Equation 5.3 is a measure that combines both precision and recall and is generally described as a harmonic mean of the two. The idea behind this metric is to have a way to measure the two ratios, Precision and Recall, in a balanced way. This is a very useful method because it balances the two previously calculated metrics, which in effect combines many of the other aspects into a single overall score. [26]

$$F_1 = 2 \cdot \frac{\text{precision} \cdot \text{recall}}{\text{precision} + \text{recall}} = \frac{2TP}{2TP + FP + FN} \quad (5.3)$$

Table 5.4: Noise study summary for Signal-Based algorithm.

Noise power $\text{mag}^2/(\text{rad}/\text{sec})$	TP	TN	FP	FN
0.1	17	99	1	3
1	16	100	0	4
10	8	100	0	12
20	8	100	1	11
50	8	95	5	12

		Actual Values	
		Positive	Negative
Predicted Values	Positive	True Positives	False Positives
	Negative	False Negatives	True Negatives

Figure 5.8: Confusion Matrix.

Table 5.5: Confusion Matrix for Signal-Based algorithm.

		Actual Condition	
		Positive	Negative
Predicted Condition	Positive	57	42
	Negative	7	494

Table 5.6: Confusion Matrix for DT with fixed irradiance.

		Actual Condition	
		Positive	Negative
Predicted Condition	Positive	66	31
	Negative	6	497

Table 5.7: Comparison between methods of Fault Diagnosis

	Recall	Precision	F1-Score
Signal-Based	0.890	0.576	0.699
Digital Twin	0.917	0.680	0.781

Table 5.7 shows the results obtained for each metric for both algorithms. As expected, the DT performs better for each metric, making it clearly the superior method.

Chapter 6

Conclusion and Future Work

6.1 Conclusion

In this dissertation, an approach for a faster and more reliable fault diagnosis in DC-DC converters for photovoltaic applications has been proposed, analysed and developed. This project is able not only to identify different types of faults, but also to distinguish between them based on several diagnostic variables involved in the PV system. Moreover, a signal-based algorithm has been developed as a comparison term based on a similar approach found in the current state of the art.

The system and its faults were modelled in MATLAB Simulink, as this is a very powerful tool that allows the work to run smoothly and without failure. An initialization script was created as a tool to have a simpler and more accessible way to implement the fault and run the simulations with simple inputs that are very convenient for the user. This proved to be very useful throughout the work as it significantly reduced the time needed to analyse the data and create the algorithms.

Once the selected faults were successfully modelled and the behaviour obtained met the expectations of the research conducted prior to the start of the project, each available variable was analysed to determine which ones could be selected as diagnostic variables that had a reasonably linear progression and could be translated into a function related to either the selected load or irradiance. Each algorithm was able to successfully identify each fault, with minor exceptions for faults in the MPPT algorithm when the optimal duty cycle is close to its default value. A study developed for the operation of the PV system in its optimal condition showed that the MPPT algorithm was able to operate between a load of 17 and 58 Ω , and the algorithm was developed for these conditions.

Adding white noise to the diagnostic variables was the chosen method for evaluating the strength of the algorithm, as the success rate without this noise was close to the maximum possible. As expected, a digital twin approach was more successful than a traditional signal-based algorithm, being superior in all chosen metrics. While the DT approach achieved a Recall of 0.891, a Precision of 0.68, and an F1-Score of 0.781, the signal-based algorithm achieved worse but satisfactory results of 0.891, 0.576, and 0.7 in the respective metrics.

These results suggest that although DT is a more expensive and complex method of fault diagnosis, for this application it should still be seriously considered if the converter in question is of major importance and its failure will have significant consequences.

6.2 Future Work

The work carried out in this dissertation has provided a foundation on the basis of a digital twin and method to develop successful fault diagnosis algorithms. However, further work should be carried as this project was conducted in a completely theoretical environment and should be tested in a real physical system.

Also, the frequently mentioned undesirable variables, which are sometimes very difficult to measure, should be the subject of further investigation, and a method for their removal or replacement from the algorithms should be explored.

The DT developed in this project is also not ideal, as it is very computationally intensive, and a simpler method of modeling the physical system should be obtained. However, since there was no real physical system in this project, the method applied can be used as a guide for creating a DT for fault diagnosis of DC-DC converters.

References

- [1] Manel Hlaili and Hfaiedh Mechergui. Comparison of different mppt algorithms with a proposed one using a power estimator for grid connected pv systems. *International Journal of Photoenergy*, 2016, 2016. doi:10.1155/2016/1728398.
- [2] Ehsan Jamshidpour, Philippe Poure, and Shahrokh Saadate. Photovoltaic systems reliability improvement by real-time fpga-based switch failure diagnosis and fault-tolerant dc-dc converter. *IEEE Transactions on Industrial Electronics*, 62:7247–7255, 11 2015. doi:10.1109/TIE.2015.2421880.
- [3] Photovoltaic energy factsheet | center for sustainable systems. URL: <https://css.umich.edu/factsheets/photovoltaic-energy-factsheet>.
- [4] Eunice Ribeiro, Antonio J.Marques Cardoso, and Chiara Boccaletti. Fault-tolerant strategy for a photovoltaic dc-dc converter. *IEEE Transactions on Power Electronics*, 28:3008–3018, 2013. doi:10.1109/TPEL.2012.2226059.
- [5] E. H. Glaessgen and D. S. Stargel. The digital twin paradigm for future nasa and u.s. air force vehicles. *Collection of Technical Papers - AIAA/ASME/ASCE/AHS/ASC Structures, Structural Dynamics and Materials Conference*, 2012. doi:10.2514/6.2012-1818.
- [6] Solar photovoltaic cell basics | department of energy. URL: <https://www.energy.gov/eere/solar/solar-photovoltaic-cell-basics>.
- [7] Eunice De Fátima and Fragoso Ribeiro. Fault diagnosis in energy systems for telecommunications. 2014. URL: <https://estudogeral.uc.pt/handle/10316/24183>.
- [8] Xuan Hieu Nguyen and Minh Phuong Nguyen. Mathematical modeling of photovoltaic cell/module/arrays with tags in matlab/simulink. *Environmental Systems Research*, 4, 12 2015. doi:10.1186/S40068-015-0047-9.
- [9] Information on solar photovoltaic stand-alone, grid connected hybrid systems. URL: <http://www.synergyenviron.com/resources/solar-photovoltaic-systems>.
- [10] Jacob James Nedumgatt, K. B. Jayakrishnan, S. Umashankar, D. Vijayakumar, and D. P. Kothari. Perturb and observe mppt algorithm for solar pv systems-modeling and simulation. *Proceedings - 2011 Annual IEEE India Conference: Engineering Sustainable Solutions, INDICON-2011*, 2011. doi:10.1109/INDCON.2011.6139513.
- [11] Venkata Guru Raghavendra Kummara, Kamran Zeb, Anand Muthusamy, T. N.V. Krishna, S. V.S.V. Prabhudeva Kumar, Do Hyun Kim, Min Soo Kim, Hwan Gyu Cho, and Hee Je Kim. A comprehensive review of dc–dc converter topologies and modulation strategies with recent advances in solar photovoltaic systems. *Electronics (Switzerland)*, 9, 1 2020. doi:10.3390/ELECTRONICS9010031.

- [12] Rui Wu, Frede Blaabjerg, Huai Wang, Marco Liserre, and Francesco Iannuzzo. Catastrophic failure and fault-tolerant design of igbt power electronic converters - an overview. *IECON Proceedings (Industrial Electronics Conference)*, pages 507–513, 2013. doi:10.1109/IECON.2013.6699187.
- [13] Fernando Bento and Antonio J. Marques Cardoso. A comprehensive survey on fault diagnosis and fault tolerance of dc-dc converters. *Chinese Journal of Electrical Engineering*, 4:1–12, 9 2018. doi:10.23919/CJEE.2018.8471284.
- [14] Ahsan Mehmood, Hadeed Ahmed Sher, Ali Faisal Murtaza, and Kamal Al-Haddad. Fault detection, classification and localization algorithm for photovoltaic array. *IEEE Transactions on Energy Conversion*, 36:2945–2955, 12 2021. doi:10.1109/TEC.2021.3062049.
- [15] Palak Jain, Jason Poon, Jai Prakash Singh, Costas Spanos, Seth R. Sanders, and Sanjib Kumar Panda. A digital twin approach for fault diagnosis in distributed photovoltaic systems. *IEEE Transactions on Power Electronics*, 35:940–956, 1 2020. doi:10.1109/TPEL.2019.2911594.
- [16] Ehsan Jamshidpour, Philippe Poure, and Shahrokh Saadate. Common switch fault diagnosis for two-stage dc-dc converters used in energy harvesting applications. *Electronics 2019, Vol. 8, Page 293*, 8:293, 3 2019. URL: <https://www.mdpi.com/2079-9292/8/3/293/html><https://www.mdpi.com/2079-9292/8/3/293>, doi:10.3390/ELECTRONICS8030293.
- [17] Weifei Hu, Tongzhou Zhang, Xiaoyu Deng, Zhenyu Liu, and Jianrong Tan. Digital twin: a state-of-the-art review of its enabling technologies, applications and challenges. *Journal of Intelligent Manufacturing and Special Equipment*, 2:1–34, 8 2021. doi:10.1108/JIMSE-12-2020-010.
- [18] EnergyPal. Solar panel guide specification data sheet.
- [19] Faq: Causes of electrical cable failure | eland cables. URL: <https://www.elandcables.com/the-cable-lab/faqs/faq-what-are-the-main-causes-of-electrical-cable-failure>.
- [20] Mingxuan Chen, Suliang Ma, Jianwen Wu, and Lian Huang. Analysis of mppt failure and development of an augmented nonlinear controller for mppt of photovoltaic systems under partial shading conditions. *Applied Sciences (Switzerland)*, 7, 2017. doi:10.3390/APP7010095.
- [21] Levy Ferreira Costa and Marco Liserre. Failure analysis of the dc-dc converter: A comprehensive survey of faults and solutions for improving reliability. *IEEE Power Electronics Magazine*, 5:42–51, 12 2018. doi:10.1109/PEL.2018.2874345.
- [22] Tamer Kamel, Yevgen Biletskiy, Christopher P. Diduh, and Liuchen Chang. Fault diagnoses for all the stages of the power electronic converter. *2012 25th IEEE Canadian Conference on Electrical and Computer Engineering: Vision for a Greener Future, CCECE 2012*, 2012. doi:10.1109/CCECE.2012.6334990.
- [23] Ahmad K. Sleiti, Jayanta S. Kapat, and Ladislav Vesely. Digital twin in energy industry: Proposed robust digital twin for power plant and other complex capital-intensive large engineering systems. *Energy Reports*, 8:3704–3726, 11 2022. doi:10.1016/J.EGYR.2022.02.305.

- [24] Introduce white noise into continuous system - simulink. URL: <https://www.mathworks.com/help/simulink/slref/bandlimitedwhitenoise.html>.
- [25] Understanding confusion matrix | by sarang narkhede | towards data science. URL: <https://towardsdatascience.com/understanding-confusion-matrix-a9ad42dcfd62>.
- [26] A look at precision, recall, and f1-score | by teemu kanstrén | towards data science. URL: <https://towardsdatascience.com/a-look-at-precision-recall-and-f1-score-36b5fd0dd3ec>.